AN ABSTRACT OF THE THESIS OF

Saleh N. Alhajeri for the degree of Master of Science in Mechanical Engineering presented on May 2, 2002.
Title: Large-Strain Softening of Aluminum in Shear at Elevated Temperature.

Abstract approved: Redacted for privacy
Michael E. Kassner

Pure aluminum deformed in torsion (shear) at elevated temperatures reaches a broad "peak" stress and then undergoes about a 17% decrease in flow stress with deformation to roughly 1-2 equivalent uniaxial strain. Beyond this strain the flow stress is approximately constant. The sources for this softening are unclear. The suggested basis includes texture softening, microstructural softening, and enhanced dynamic recovery. Experiments were performed where specimens were deformed in torsion to various strains within the softening regime followed by compression tests at ambient and elevated temperature. Analysis of the compressive yield strengths indicate that the softening is at least substantially explained by a decrease in the average Taylor factor due to the development of texture.

Large-Strain Softening of Aluminum in Shear at Elevated Temperature

by
Saleh N. Alhajeri

A THESIS

submitted to

Oregon State University

in partial fulfillment of
the requirements for the
degree of

Master of Science

Presented May 2, 2002
Commencement June 2002

Master of Science thesis of Saleh N. Alhajeri presented on May 2, 2002.

APPROVED:

Redacted for privacy

Major Professor, representing Mechanical Engineering

Redacted for privacy

Head of the Department of Mechanical Engineering

Redacted for privacy

Dean of the Graduate School

I understand that my thesis will become part of the permanent collection of Oregon State University libraries. My signature below authorizes release of my thesis to any reader upon request.

Redacted for privacy

Saleh N. Alhajeri

ACKNOWLEDGMENTS

I would like to express my sincere appreciation to the following people whom without their support this thesis would not have been possible. It is a pleasure to recognize and thank those who supported me.

I would like to thank the Public Authority for Applied Education and Training-Kuwait for their financial support throughout the duration of my Master's program.

Special thanks are extended to my advisor, Dr. Michael E. Kassner, for his invaluable guidance, support, and advice throughout this research. His leadership and training became the building blocks which helped me understand the foundations of scientific research. I would also like to thank Dr. Ming Wang for his invaluable help and advice.

I would like to express my gratitude to my committee members, Dr. Timothy C. Kennedy, Dr. William H. Warnes, and Dr. R. Logen Logendran. I appreciate their time investment and their advice.

Finally, I would like to thank my mother for always believing in me. Without her support and love I would never achieved this. I would also like to thank my dear wife for her unconditional love and patience. Her sacrefices have been greatly appreciated.

TABLE OF CONTENTS

LIST OF FIGURES

LIST OF FIGURES (Continued)

LARGE-STRAIN SOFTENING OF ALUMINUM IN SHEAR AT ELEVATED TEMPERATURE

1. INTRODUCTION

The stress versus strain behavior and microstructural evolution of aluminum deformed in pure shear (e.g., torsion) at elevated temperatures has been studied by a variety of groups including Myshlyaev and coworkers [1-4], Montheillet and coworkers [5-7], McQueen and coworkers [8-12], Pettersen [13,14], and Kassner and coworkers [15-19].

The ductility of high and commercial purity aluminum and some aluminum alloys can exceed, in torsion, equivalent uniaxial strains of 100. Typically, the Al hardens to a peak stress, $\overline{\sigma}_{p,ss}$, at strains less than 0.5. The flow stress subsequently decreases to a flow stress, $\overline{\sigma}_{ss}$, which is nearly constant and a steady-state condition is reached. The peak stress, $\overline{\sigma}_{p,ss}$, seems essentially equivalent to the steady-state creep stress observed in tension. It is generally agreed that under pure shear, such as with torsion tests, the flow stress decreases by about 17% and this occurs over a fairly broad range of strain of 1-2, depending on the temperature and strain rate. This is illustrated in Figure 1.1 [18]. This softening has not been attributed to discontinuous dynamic recrystallization (DRX) that often evinces softening in the flow behavior, rather only dynamic recovery (DRV) is widely accepted to occur. [The softening of 17% to strains of 1-2 has been noted to be followed by a slight, gradual, increase in torque (about 4%) above strains of about 10.] The cause of the softening is not fully understood.

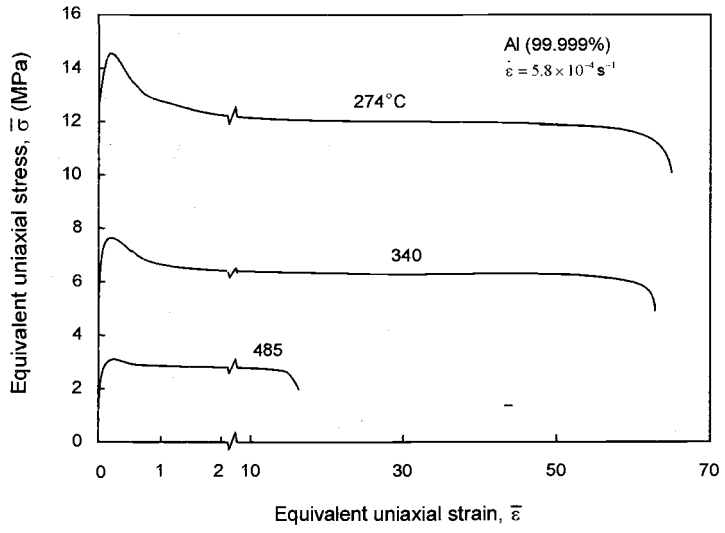

(a)

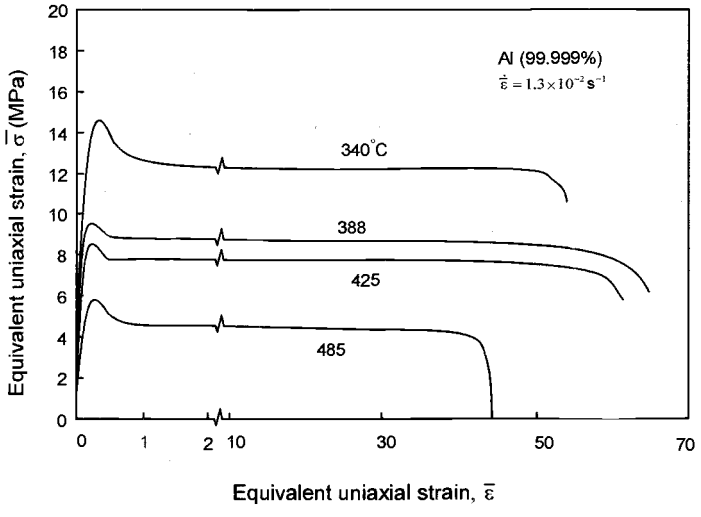

(b)

Figure 1.1: Equivalent-uniaxial stress versus equivalent-uniaxial strain of aluminum in torsion at strain rates of (a) 5.8×10^{-4} s^{-1} and (b) 1.3×10^{-2} s^{-1}.

Explanations vary from decreases in the average Taylor factor (textural softening) to changes in the dislocation substructure (e.g., increase in the average subgrain size) sometimes through increased dynamic recovery (due to increase HAB development). Furthermore, it is now widely agreed that large strain deformation results in a dramatic increase in the high-angle boundary (HAB) area. That is, one-third to one-half of the initially low-misorientation subgrain facets become HABs ($\theta > 10°$). Two groups [8-12, 15-19] attribute this primarily to geometric dynamic recrystallization (GDX), where the original grains of the polycrystalline-aggregate elongate, increase HAB area, and "replace" the subgrain boundaries with HABs. Others have considered the formation to be additionally, or primarily, due to continuous reactions (continuous dynamic recrystallization) where subgrains gradually transform to HABs resulting from dislocation accumulation [5-7,13]. The formation of HABs in single crystals was confirmed to occur in Al at high temperatures and not as a consequence of DRX [19]. Thus, HABs can form in some cases from dislocation reaction. The number of HABs in the single crystal, however, was much less than for large strain deformation of polycrystals to identical large strains. Thus, GDX may be more important in terms of forming HABs, at least in pure polycrystalline aluminum. Geometric necessary boundaries (GNBs) are HABs that form from dislocation reaction and occur as incompatible slip occurs in a given grain/crystal, Figure 1.2, [20].

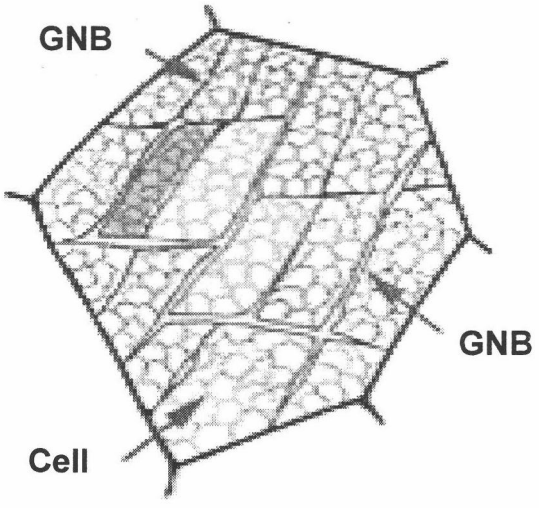

Figure 1.2: Schematic of a grain showing the geometric necessary boundaries (GNBs) [23].

Pettersen [13] recently suggested that the softening in aluminum alloys (AA 6060 and 6082) is a result of these new HABs being particularly effective sinks or annihilation sites for dislocations leading to softening from larger subgrain sizes. More specifically, the softening is due to a combination of factors, including decrease in strength due to a decrease in the average Taylor factor, as well as to changes in the size of the subgrains. One problem with this analysis is that it appears that changes in the subgrain size in Al, by itself, do not seem to affect the flow stress, as discussed extensively in [21]. Pettersen also suggested that a significant fraction of the boundaries formed from dislocation reactions such as with GNBs.

The softening has not been attributed to any new deformation mechanism that might arise from the increase in HAB area, such as Coble creep or an increased contribution to strain from grain boundary sliding (GBS). This is largely due to the fact that the activation energy for creep-plasticity is unchanged from that of self-

diffusion, and the stress exponent is unchanged from that of about 4-5. Either Coble or GBS would be associated with smaller stress exponents (1-2) and activation energies about half that of lattice self-diffusion.

Pettersen found that the textures and corresponding Taylor factors (M) for some hot-deformed aluminum alloys were, based on x-rays and orientation image maps (OIMs), principally:

Texture Component	Texture Orientation	Taylor Factor
A^2	$\{\bar{1}\,\bar{1}1\}<112>$ and $\{11\bar{1}\}<112>$	—
C	$\{001\}$ <110>	2.65
B^1	$\{\bar{1}12\}<110>$ and $\{1\bar{1}\,\bar{2}\}<\bar{1}\,\bar{1}0>$	2.34
Isotropic	—	2.69

where A^2 was observed to be relatively weak. Pettersen based the above Taylor factors on slip on non-traditional systems. The first index is the shear plane and the second is the shear direction.

McQueen [12] only observed the strong B^1 texture based on x-ray diffraction and STEM on pure aluminum. Shrivastava *et. al* [22] calculated the torsional Taylor factor using the Bishop and Hill (traditional slip systems) method for each of these three textures. The average value was 2.39, or about 16% less than 2.86 for a random array of aggregates. If the strongest (B^1) texture is used, and the "traditional" Taylor factors are used, a decrease in Taylor factor from 2.86 to 2.44 is expected, leading to a flow stress decrease of 15%. This kind of analysis was performed by Perdrix *et al.* [5] on aluminum with a similar result. Pettersen argued that the "harder" C component texture that she observed in addition to the B^1

texture in the aluminum alloy only mandated a decrease in flow stress of 5-7%, with, again, the remaining softening resulting from increased dynamic recovery.

The purpose of the work in the present investigation is to assess the contribution of the texture (average Taylor factor) on the softening behavior. This will be accomplished by performing compression tests subsequent to torsion tests to various strains within the softening regime. If microstructural effects rationalize the torsion softening, then the compressive yield stress will decrease with torsional prestrain. However, Taylor factor analysis reveals that if textures are responsible for the softening, the compressive (compression axis parallel to torsion axis) yield stresses will be approximately unchanged with torsion prestrains.

2. LITERATURE REVIEW

Belyayev *et al.* (1981) investigated the behavior of aluminum (99.92 % purity) under torsion [1], and during creep in "superplasticity conditions" [2]. Results showed that dynamic recrystallization (DRX) occurs at temperatures below 350°C at high levels of deformation. They concluded that the stage of superplastic flow is a result of continuous dynamic recrystallization in-situ, a process which is continually freeing the metal of defects and thus providing the possibility of practically unlimited deformation.

Likhachev *et al.* (1981) studied the properties of the mechanical behavior of aluminum in the course of its active deformation and creep strain, features of the development of structure in these regimes and the effect of temperature and force conditions of deformation on these processes in the region of "superplasticity" [3]. Based on the experimental data, they concluded that the very high plasticity of aluminum seen at 450°C is the result of suppression of destructive processes owing to an intensification of accommodation channels of various kinds and predominance of the dynamic activity of elements of the defect structure over the competing processes of diffusion pore formation. The same group (1985) studied the specific features of the mechanical behavior, the evolution of the microstructure, and the fracture kinetics of aluminum under the "superplastic" conditions [4]. Different aluminum specimens (99.999%, 99.92%, 99.5%, and 93.3% purity) were deformed under torsion at different strain rates. The same results as reported in [1] and [2] were found in this investigation. In the above cases, the term "superplasticity" is implied in the 5-power law regime and does not reflect the GBS usually associated with (2-power) "conventional" superplasticity.

Torsion tests were performed by Perdrix *et al.* (1981) over the range of temperatures between 400 and 550°C on commercial aluminum samples and two

alloys Al-Mg and Al-Mn with deformations to strains in excess of $\bar{\varepsilon}$ = 30 [5]. Results showed that the dynamic restoration process only results in a stationary regime for extremely large deformations. They concluded that the decrease in the flow stress during the course of the deformation is explained by the change in structure and the crystallographic texture of the material. They also concluded that the increase in high-angle boundary area was a consequence of "continuous reactions".

Uniaxial compression tests were carried out by Gourdet *et al.* (1996) on aluminum, single and polycrystals [6]. They concluded that continuous dynamic recrystallization (CDX) occurs in single crystal, whereas both CDX and geometric dynamic recrystallization (GDX) operate simultaneously in polycrystals. Torsion and uniaxial compression tests were also carried out by Gourdet and Montheillet (2000) on aluminum, single and polycrystals [7]. They concluded that subgrain boundaries of the single crystalline samples can effectively transform into grain boundaries, especially when the initial orientation is unstable. In the case of the polycrystalline specimens, it was found that continuous dynamic recrystallization (CDX) operates faster in the commercial purity aluminum compared to the pure aluminum and Al-Mg alloy.

McQueen *et al.* (1985) investigated the behavior of aluminum (99.7 % purity) under torsion [8]. Results showed that the flow stress, subgrain size and misorientation remain substantially constant over strains from 1 to 60 with a decline in steady state stress due to development of a soft structure. Grains become elongated but remain distinguishable as long as their thickness is greater than the subgrain diameter. However, the grains develop serrations and become pinched off when average thickness fall below the subgrain size. Solberg *et al.* (1989) as a continuation of the latter study, investigated the behavior of aluminum (99.7 % purity) under torsion [9]. Results showed that the grains wound into helicoids with

an axial thickness varying inversely with the strain. Subgrains persisted at a constant size and equiaxed throughout the straining from 0.5 to 60. The grains, with their boundaries strongly serrated, retained their distinctness up to strains of 10 for 0.1 mm grains and up to 60 for 2 mm grains, while their thickness was greater than the subgrain diameter. For the former at strains of 20-60, the microstructure consists of subgrains having a mixture of small- and large-angle boundaries. This development is the geometric dynamic recrystallization (GDX). McQueen *et al.* (1991) supported the theory that dynamic recovery (DRV) is the principal restoration mechanism in dilute aluminum alloys ($\leq$ 3 % Mg) and that dynamic recrystallization (DRX) is absent [10]. Observations of DRX in more concentrated alloys, notably when particle enhancement is involved, appear to be valid.

Textures have been measured by McQueen (1999) over the range 20 to 840°C after a series of torsional strains extending as high as $\varepsilon = 60$ in aluminum polycrystals [12]. Results showed that texture of aluminum underwent a transition near $\varepsilon = 10$ as a result of relaxation of the grain edge constraints; this caused a reduction of the Taylor factor. The aluminum underwent only dynamic recovery but at high strains the serrated grain boundaries met, thus pinching-off the grains into short segments in the process of geometric dynamic recrystallization (GDX).

Kassner and McMahon (1987) studied the behavior of aluminum of 99.999% purity under torsion at 371°C and an equivalent uniaxial strain rate of 5.04×10^{-4} s^{-1} to various steady-state strains up to 16.33 [16]. Results showed that the subgrain size and density of dislocations not associated with boundaries remained fixed throughout the wide steady-state strain range. The subgrain boundaries, however, underwent two important changes. At the onset of steady state ($\varepsilon \approx 0.2$) all of the subgrain boundaries had relatively small misorientation angles averaging about 0.5 deg. With increased strain, however, an increasing fraction of the subgrain facets were high-angle boundaries. At strains greater than

about four nearly a third of the boundaries were high-angle. In specimens with both types of boundaries, the high-angle boundaries have misorientation angles (θ) greater than 10 degrees, while θ for low-angle boundaries is nearly always less than 3 degrees. Only rarely do subgrain boundaries have misorientation angles between 3 and 10 degrees. In aluminum, the increased high-angle boundary area at larger strains originates from the extension of the initial boundaries through the mechanism of geometric dynamic recrystallization (GDX). The average misorientation across low-angle boundaries initially increases during steady state but eventually reaches a maximum value of about 1.2 degrees at $\varepsilon \approx 1.2$.

The torsional ductility of high purity aluminum was measured by Kassner *et al.* (1991) over a wide range of temperature and strain [18]. At each strain rate the ductility first increases with increasing temperature to a "peak ductility", beyond which it decreases. Dramatic ductilities, of over 90 in some cases, are observed in the vicinity of the peaks. The peak ductility appears to increase with increasing strain rate. The temperature at which the peak ductility is observed increases with increasing strain rate, Figure 2.1. At temperatures below the peak, as temperature rises, dynamic recovery mitigates internal stresses and may retard crack nucleation to produce improved ductility. Increased strain rate at a given temperature increases the internal stresses and the ductility decreases. At temperatures above the peak, diffusive void formation reduces the ductility. Consequently, increased strain rate raises the amount of torsional strain relative to the increase in cavity growth rate and the ductility increases.

Kassner (1998) studied the behavior of aluminum single crystals (99.999 % purity) under torsion to strains over 16 at 391°C [19]. Some high angle boundaries formed, but there is no evidence of discontinuous dynamic recrystallization,

consistent with high purity polycrystal results above 274°C. Furthermore, the results confirm the concept of geometric dynamic recrystallization.

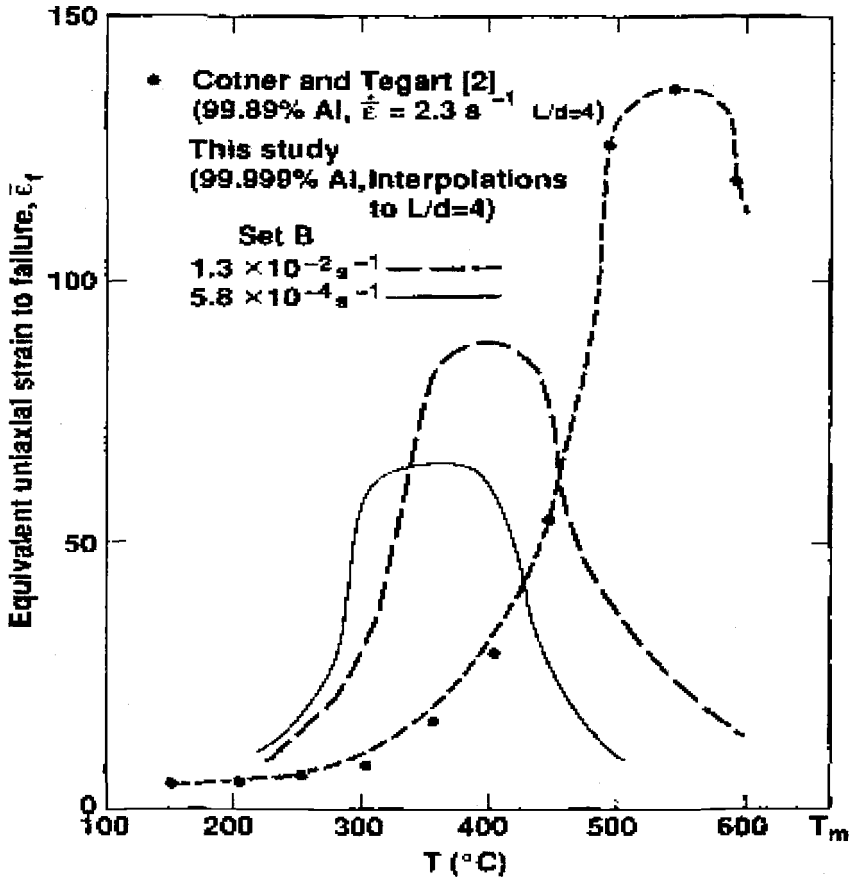

Figure 2.1: Variation of the torsional ductility of 99.999% aluminum with temperature at three different strain rates [18].

3. RECRYSTALLIZATION

3.1 INTRODUCTION

During deformation, energy is stored in the material mainly in the form of dislocations [23]. This energy is released in three main processes, those of recovery, recrystallization, and grain coarsening (subsequent to recrystallization). The usual definition of recrystallization is the formation of a new grain structure in a deformed material by the formation and migration of high angle grain boundaries driven by the stored energy of deformation. High angle grain boundaries are those with greater than a 10-15° misorientation. Recovery can be defined as all annealing processes occurring in deformed materials that occur without the migration of a high angle grain boundary. Typically, recovery processes involve the rearrangement of dislocations to lower their energy, for example by the formation of low-angle subgrain boundaries, and annihilation of dislocation line length in the subgrain interior, such as by Frank network coarsening. Grain coarsening can, in turn, be defined as the growth of the mean grain size driven by the reduction in grain boundary area. Coarsening can occur by either "normal" grain growth, whose main mechanism is the disappearance of the smallest grains in the distribution, or "abnormal" grain growth. The latter process involves the growth of a few grains which become much larger than the average. This is illustrated in Figure 3.1.

The process of recrystallization of plastically deformed metals and alloys is of central importance in the processing of metallic alloys for two main reasons. The first is to soften and restore the ductility of material hardened by low temperature deformation (that occurring below about 50% of the absolute melting temperature, $0.5T_m$). The second is to control the grain structure of the final product. For many metallic alloys, especially those based on copper, nickel, and aluminum, recrystallization after deformation is the only method for producing a completely

new grain structure with a modified grain size, shape, and, in particular, mean orientation or texture.

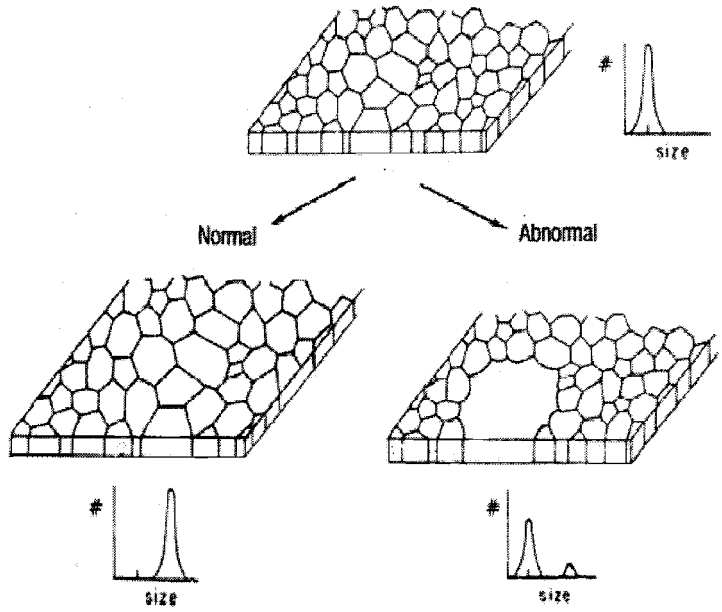

Figure 3.1: Schematic drawing showing the difference between normal and abnormal grain growth.

It is now recognized that recrystallization is not a Gibbs I transformation that occurs by classic nucleation and growth process [23, 24]. ΔG^* and r^*, the critical Gibb's free energy and critical-sized embryos, are unrealistically large if the proper thermodynamic variables are used. As a result of this disagreement, it is now universally accepted that the new grains do not nucleate as totally new grains by the atom-by atom construction assumed in the classic kinetic models. Rather, new grains grow from small regions, such as subgrains, that are already present in the deformed microstructure. Special grains do not have to form. These embryos

are present in the starting structure. Only subgrains with a high misorientation angle to the adjacent deformed material appear to have the necessary mobility to evolve into new recrystallized grains. Typical nucleation sites include pre-existing high angle boundaries, shear bands, and highly misoriented deformation zones around hard particles. Misoriented "transition" bands (or geometric necessary boundaries) inside grains are a result of different parts of the grain having undergone different lattice rotations due to different slip systems being activated. Figure 3.2 illustrates an example of recrystallization in 40% compressed pure aluminum. New grains 3 and 17 are only growing into the deformed regions A and B, respectively, with which they are strongly misoriented and not into regions with which they share a common misorientation; 17 has a low angle misorientation with A and 3 with B. It should be mentioned that recrystallization often leads to a characteristic texture(s), different than any texture developed as a consequence of the prior deformation, that is the driving force for any recrystallization.

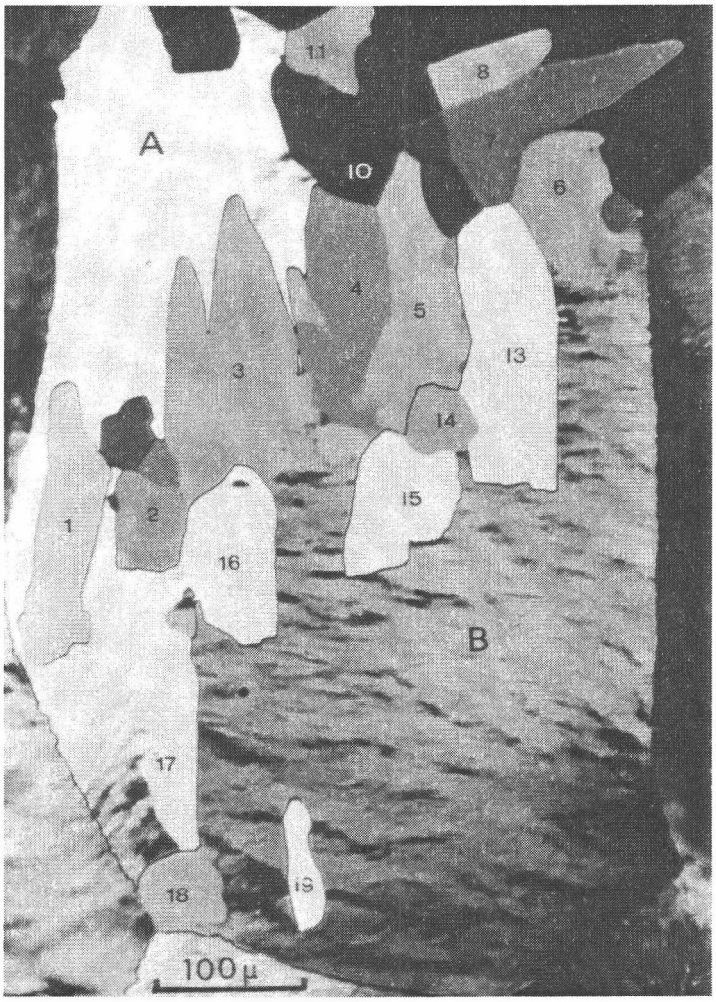

Figure 3.2: Optical micrograph of partially recrystallized coarse grained pure aluminum compressed 40% [23].

3.2 DISCONTINUOUS DYNAMIC RECRYSTALLIZATION (DRX)

Recrystallization can occur under two broad conditions; static and dynamic. Basically, static occurs in the absence of external plasticity during the recrystallization [24]. The most common case for static is heating cold-worked metal leading to a recrystallized microstructure. Dynamic recrystallization occurs with concomitant plasticity. This distinction is complicated, somewhat, by the more recent suggestion of metadynamic recrystallization (MDRX) that can follow dynamic recrystallization, generally at elevated temperature. Although it occurs without external plasticity, it can occur quickly (e.g., during deformation passes at high temperatures). It is distinguished from static recrystallization (SRX) in that MDRX is relatively sensitive to prior strain rate but insensitive to prestrain and temperature. Static recrystallization depends on prestrain and temperature, but only slightly on strain rate. The recrystallization remarks in the previous section are equally valid for these two cases (although Figure 3.2 was a static recrystallization example) although differences are apparent.

Figure 3.3(a) illustrates the stress versus strain curve of pure (99.9%) zirconium undergoing conventional discontinuous dynamic recrystallization. A single broad stress peak, where the material hardens to a peak stress, is followed by significant softening. The softening is largely attributable to the nucleation of growing, "new," grains that annihilate dislocations during growth. The restoration is contrasted by dynamic recovery, where the movement of, and annihilation of, dislocations at high angle boundaries is not important. Figure 3.3(b) does not evince DRX. Stage IV hardening (constant hardening rate) that precludes saturation, is also observed. DRX may commence well before the peak stress. This becomes evident without microstructural examination by examining the hardening rate, θ, as a function of flow stress.

Sometimes the single peak in the stress versus strain behavior of Figure 3.3(a) for DRX is not observed; rather multiple peaks may be evident leading to the appearance of undulations in the stress versus strain behavior that "dampen" into an effective "steady-state." This is illustrated in Figure 3.4. It has been suggested that the cyclic behavior indicates that grain coarsening is occurring while a single peak is associated with grain refinement. Although DRX is frequently associated with commercial metal forming strain rates (e.g., 1 s^{-1} and higher), Figure 3.4 illustrates that DRX can occur at more modest rates. Metals such as pure Ni and Cu frequently exhibit DRX.

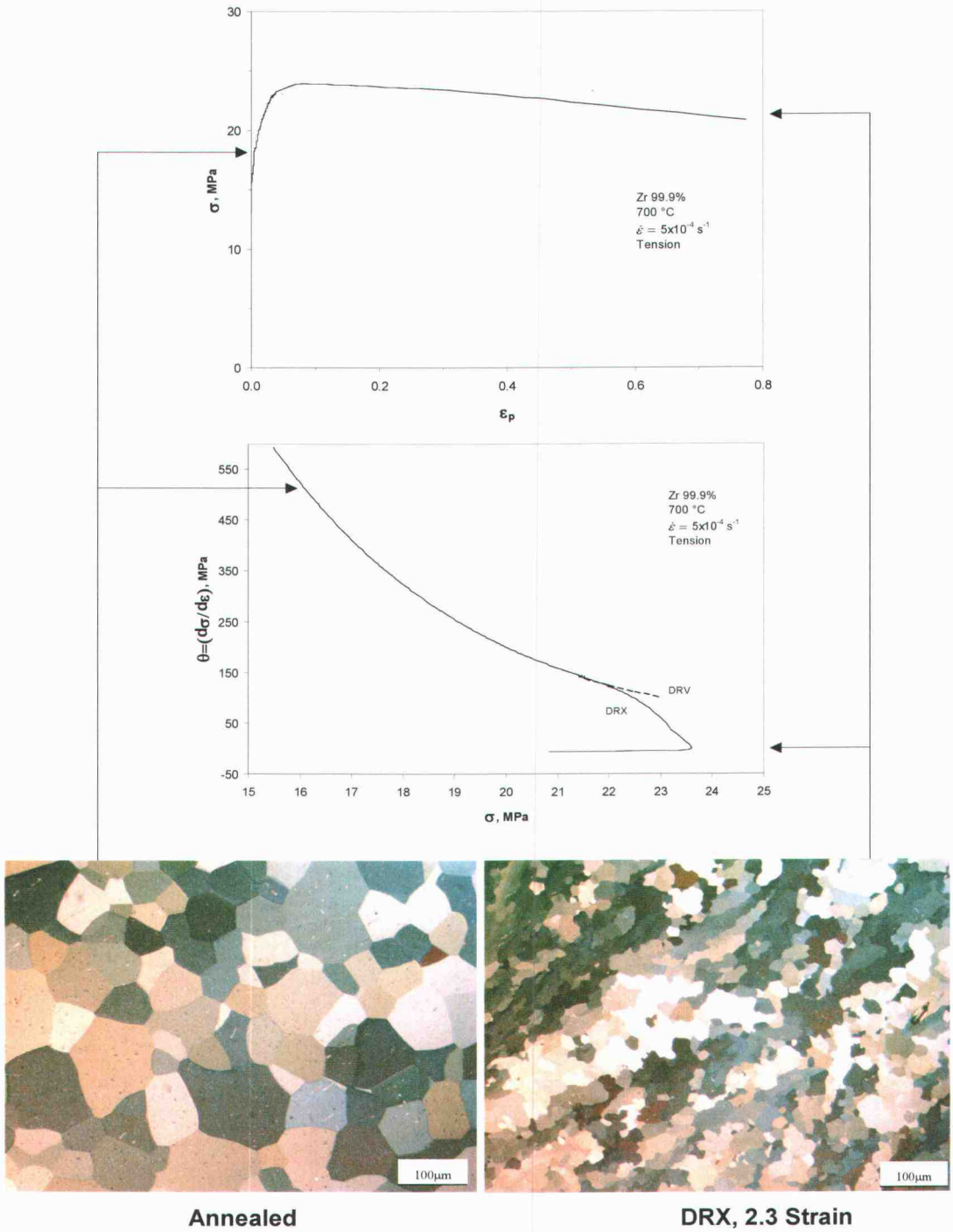

Figure 3.3(a): Pure (99.9%) zirconium undergoing conventional discontinuous dynamic recrystallization [25].

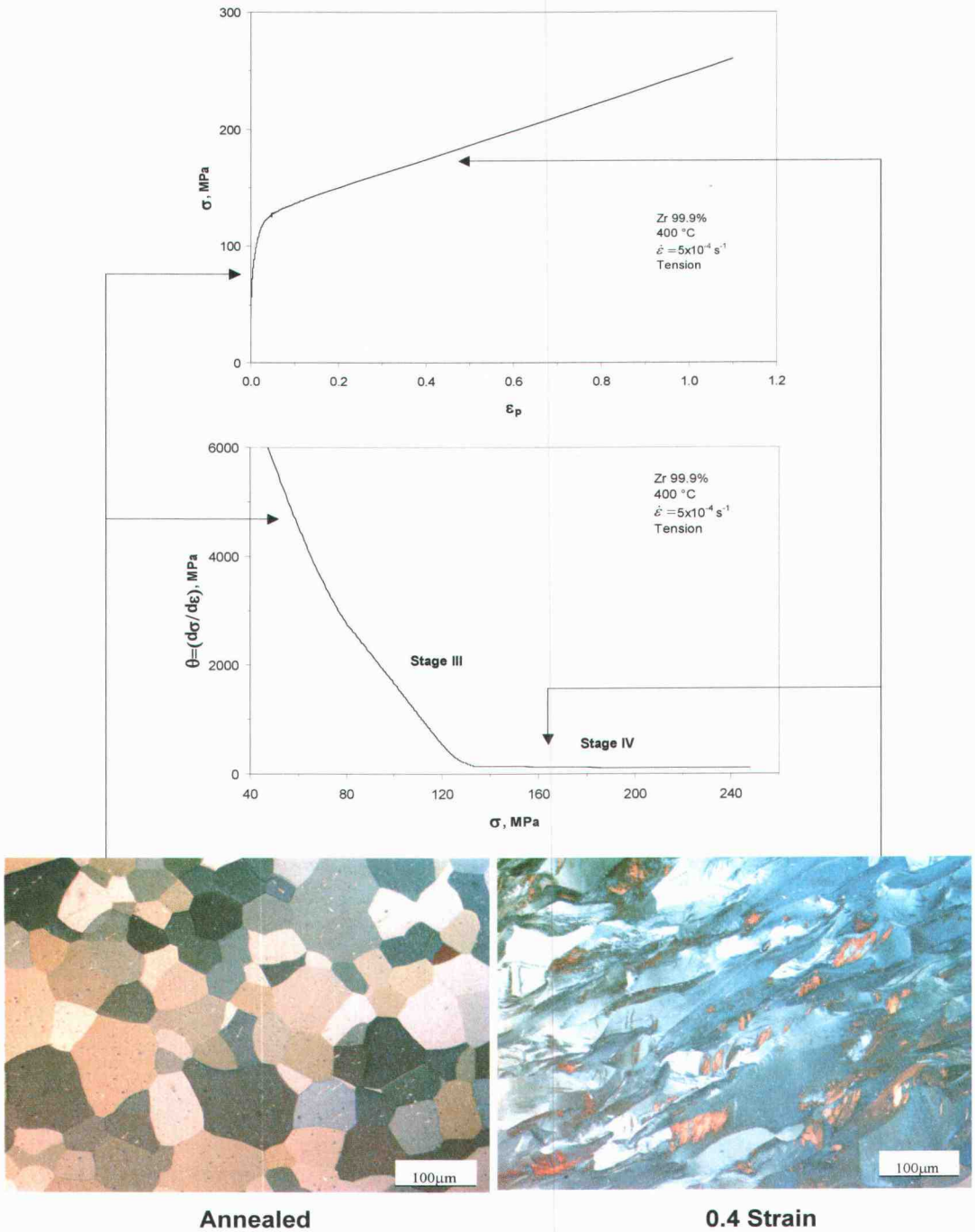

Figure 3.3(b): Pure (99.9%) zirconium that is not undergoing conventional discontinuous dynamic recrystallization [25].

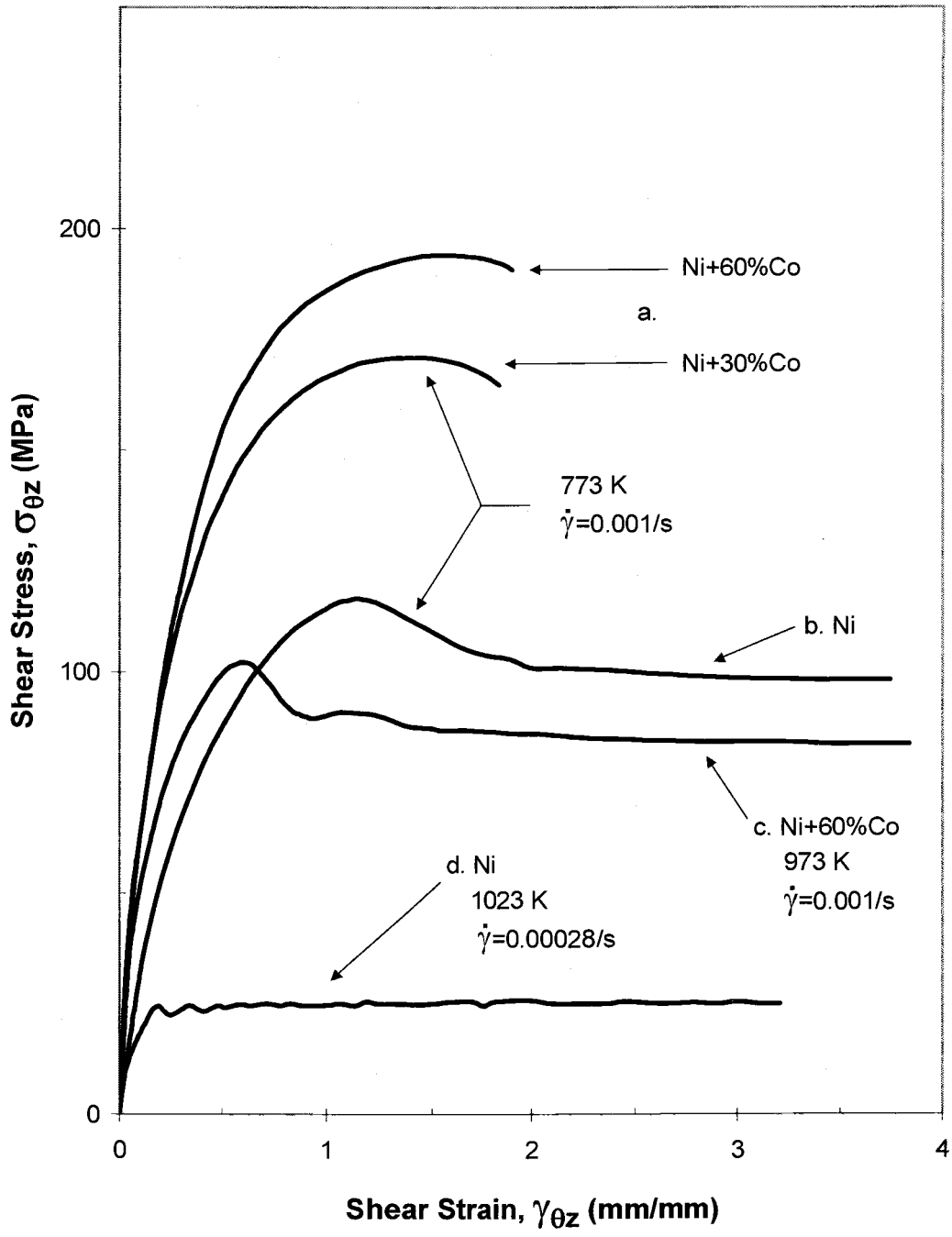

Figure 3.4: Discontinuous Dynamic Recrystallization (DRX) with a single peak and also the stress versus strain behavior that "dampens" into an effective "steady-state" [23].

3.3 GEOMETRIC DYNAMIC RECRYSTALLIZATION (GDX)

Geometric Dynamic Recrystallization (GDX) occurs at temperatures where dynamic recovery (DRV) has been observed which includes subgrain boundary formation [23, 24]. The starting grains of the polycrystalline aggregate distort with relatively large strain deformation. These boundaries may thin to the dimensions of the subgrain diameter with large strains achievable in torsion or compression. In the case of Al, the starting HABs (typically 35° misorientation) are serrated as a result of subgrain-boundary formation, presumably in association with DRV, where the typical misorientation is about a degree, or so. As the grains thin to about twice the subgrain diameter (the average subgrain size may be a factor of 10-100 less than the average diameter of the grains of the starting polycrystal), nearly a third of the subgrain facets have been replaced by high angle boundaries, which have ancestry to the starting polycrystal. The remaining two-thirds, or so, are still of low misorientation polygonized boundaries of a degree, or so. As deformation continues, "pinching off" may occur which annihilates HABs and the high angle boundary area remains constant. Thus, with GDX, the HAB area can dramatically increase but not in the same discontinuous way as DRX. Figure 3.5 illustrates the process of GDX schematically. GDX has been confused with DRX, as well and continuous reactions (discussed in a later section), but has been confirmed in Al and Al-Mg alloys, and may occur in other high stacking fault energy metals and alloys as well. Some [13, 14] have suggested that some of the HAB may result from continuous reactions or by transition bands.

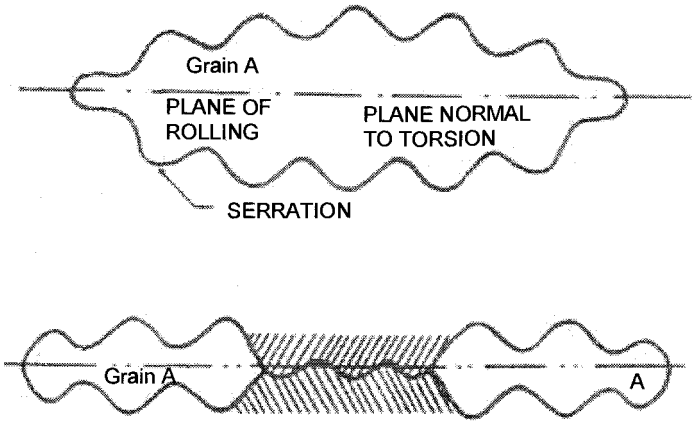

Figure 3.5: When the grains are elongated and thinned extremely, they pinch off where opposite serrations meet [23].

3.4 PARTICLE STIMULATED NUCLEATION (PSN)

An understanding of the effects of second phase particles on recrystallization is important since most industrial alloys contain second phase particles and such particles have a strong influence on the recrystallization kinetics, microstructure, and texture.

Particles are often known for their ability to impede the motions of high angle boundaries during high temperature annealing or deformation (Zener pinning). During the deformation of a particle-containing alloy, the enforced strain gradient in the vicinity of a non-deforming particle creates a region of high dislocation density and large orientation gradient (particle deformation zone or PDZ), which is an ideal site for the development of a recrystallization nucleus. The mechanisms of recrystallization in two-phase alloys do not differ from those in single phase alloys. There are not a great deal of systematic measurements of these zones, but it appears that the deformation zone may extend a diameter of the particle, or so, into the matrix and lead to misorientations of tens of degrees in the matrix, from the adjacent matrix.

3.5 CONTINUOUS REACTIONS

It is now recognized that refined grain structures may evolve homogeneously and gradually during the annealing of deformed metals, either with or without concurrent straining. This can occur even when the heterogeneous nucleation and growth stages of primary recrystallization do not occur. "Continuous reactions" is a term that is sometimes used in place of others that imply at least similar process such as "continuous recrystallization", "in-situ recrystallization" and "extended recovery." It is often observed that deformation textures sharpen and components related to the stable orientations within the prior deformation textures are retained. These observations are consistent with recovery as the sole restoration mechanism, suggesting that the terms "continuous reactions" may be more meaningful as a description than "continuous recrystallization."

Mechanisms proposed to explain the role of recovery in high angle boundary formation include subgrain growth via dislocation motion, the development of higher angle boundaries by the merging of lower angle boundaries during subgrain coalescence, and the increase of boundary misorientation through the accumulation of dislocations into the subgrain boundaries. These processes have been envisioned to result in a progressive buildup of boundary misorientation during (static or dynamic) annealing, resulting in a gradual transition in boundary character and formation of high angle grain boundaries.

4. CRYSTAL ORIENTATION

4.1 INTRODUCTION

Each grain in a polycrystalline aggregate normally has a crystallographic orientation different from that of its neighbors [26]. Considered as a whole, the orientations of all the grains may be randomly distributed in relation to some selected frame of reference, or they may tend to cluster, to a greater or lesser degree, about some particular orientation or orientations. Any aggregate characterized by the latter condition is said to have a *preferred orientation*, or *texture*, which may be defined simply as a condition in which the distribution of crystal orientations is nonrandom.

Preferred orientation is a very common condition. Among metals and alloys it is most evident in wire and sheet, and the kinds of texture found in these products are dealt with below. The preferred orientation that is produced by the forming process itself (wire drawing or sheet rolling) is called a *deformation texture*. It is due to the tendency of the grains in a polycrystalline aggregate to rotate during plastic deformation; each grain undergoes slip and rotation in a complex way that is determined by the imposed forces and by the slip and rotation of adjoining grains; the result is a preferred, nonrandom orientation. When the cold-worked metal, with a deformation texture, is recrystallized by annealing, the new grain structure usually has a preferred orientation too, often different from that of the cold-worked material. This is called a *recrystallization texture* or *annealing texture*. It is due to the influence which the texture of the cold-worked matrix has on the nucleation and/or growth of the new grains in that matrix.

Preferred orientation is not confined to metallurgical products. It also exists in rocks, ceramics, and in both natural and artificial polymeric fibers and sheets. In fact, preferred orientation is generally the rule, not the exception, and the preparation of an aggregate with completely random crystal orientations is a difficult matter.

The industrial importance of preferred orientation lies in the effect, often very marked, which it has on the overall, macroscopic properties of materials. Given the fact that some properties of single crystals are anisotropic, i.e., have different values in different directions, it follows that an aggregate having preferred orientation must also have directional properties to a greater or lesser degree. Such properties may or may not be beneficial, depending on the intended use of the material. For example, sheet steel for the cores of small electric motors should have, for magnetic reasons, all grains oriented with their {100} planes parallel to the sheet surface. But this texture would not be satisfactory if the steel were to be formed into a cup by deep drawing. Here a texture with {111} planes parallel to the surface would make the steel less likely to crack during the severe deformation of deep drawing. If the part to be formed by deep drawing has an unsymmetrical shape, a still different texture, or none at all, might yield better results. Some control of texture is possible by the proper choice of production variables such as degree of deformation and annealing temperature, but metallurgists do not yet understand texture formation well enough to produce any desired texture in any particular metal at will.

4.2 FIBER TEXTURE

The individual crystals in wire are so oriented that the same crystallographic direction [*uvw*] in most of the grains is parallel or nearly parallel to the wire axis [26]. Because a similar texture occurs in natural and artificial fibers, it is called a *fiber texture* and the axis of the wire is called the *fiber axis*. Materials having a fiber texture have rotational symmetry about an axis in the sense that all crystal orientations about this axis are equally probable, like those of beads on a string. A fiber texture is therefore to be expected in any material formed by forces that have rotational symmetry about an axis, for example, in wire and rod formed by drawing, swaging, or extrusion. Less common examples of fiber texture are sometimes found in sheet formed by simple compression, in coatings formed by hot dipping, electroplating, and evaporation, and in castings among the columnar crystals next to the mold wall. The fiber axis in these is perpendicular to the plane of the sheet or coating, and parallel to the axis of the columnar crystals.

Fiber textures vary in perfection, i.e., in the scatter of the direction [*uvw*] about the fiber axis, and both single and double fiber textures have been observed. Thus, cold-drawn aluminum wire has almost a single [111] texture, but copper, also FCC, has a double [111] + [100] texture; i.e., in drawn copper wire there are two sets of grains, the fiber axis of one set being [111] and that of the other set [100].

4.3 SHEET TEXTURE

In its simplest, most highly developed form, the texture of sheet is such that most of the grains are oriented with a certain crystallographic plane (*hkl*) roughly parallel to the sheet surface, and a certain direction [*uvw*] in that plane roughly parallel to the direction in which the sheet was rolled. Such a texture is described by the shorthand notation (*hkl*)[*uvw*]. In an ideal texture of this kind, the grain orientations in the sheet are fixed with respect to axes in the sheet; there is none of the rotational freedom of grain orientation possessed by a fiber texture.

The notation (*hkl*)[*uvw*] specifies what is called an *ideal orientation.* Some metals and alloys have sheet textures so sharp that they can be adequately described by stating the ideal orientation to which the grains of the sheet closely conform. Most sheet textures, however, have so much scatter that they can be approximated symbolically only by the sum of a number of ideal orientations or texture components, and even such a description is inadequate.

5. TAYLOR FACTOR

The most obvious effect of deformation geometry on hardening is the development of crystallographic texture [27]. Because of the crystallographic nature of slip and the general validity of Schmid's law, one expects that, at large deformations, differences in hardening may arise from purely geometric considerations. The mean inclination of the active slip planes and directions will change differently for different deformation modes. Quantitative prediction of this geometric effect has been the goal of many theoretical studies dating back to Sachs in 1924 and Taylor in 1938 [28]. Recently, several excellent reviews have been written on this topic [29, 30, 31]. Many of these reviews examined the crystallographic considerations necessary for comparing hardening for different deformation modes. They correctly point out that even at small strains (before significant texture development) crystallographic predictions of yield and flow differ from the macroscopic von Mises condition. For a randomly oriented FCC polycrystal one can relate the macroscopic stress (σ) to the critically resolved shear stress for slip (τ_c) and the macroscopic strain (ε) to the accumulated shear strain on all activated slip systems (γ_c) through the average *Taylor factor* $\overline{M}$. Specifically,

$$\sigma = \overline{M}\,\tau_c \tag{5.1}$$

$$\varepsilon = \int_0^{\gamma} \sum d\gamma_c \,/\, \overline{M} \tag{5.2}$$

The Taylor factor varies with deformation mode. Bishop and Hill showed that for tension $\overline{M}_t$ is 3.06 and for torsion $\overline{M}_\tau$ is 1.65 [32], Figure 5.1. The Taylor factors

clearly vary/evolve with strain; differently with each of the three deformation modes.

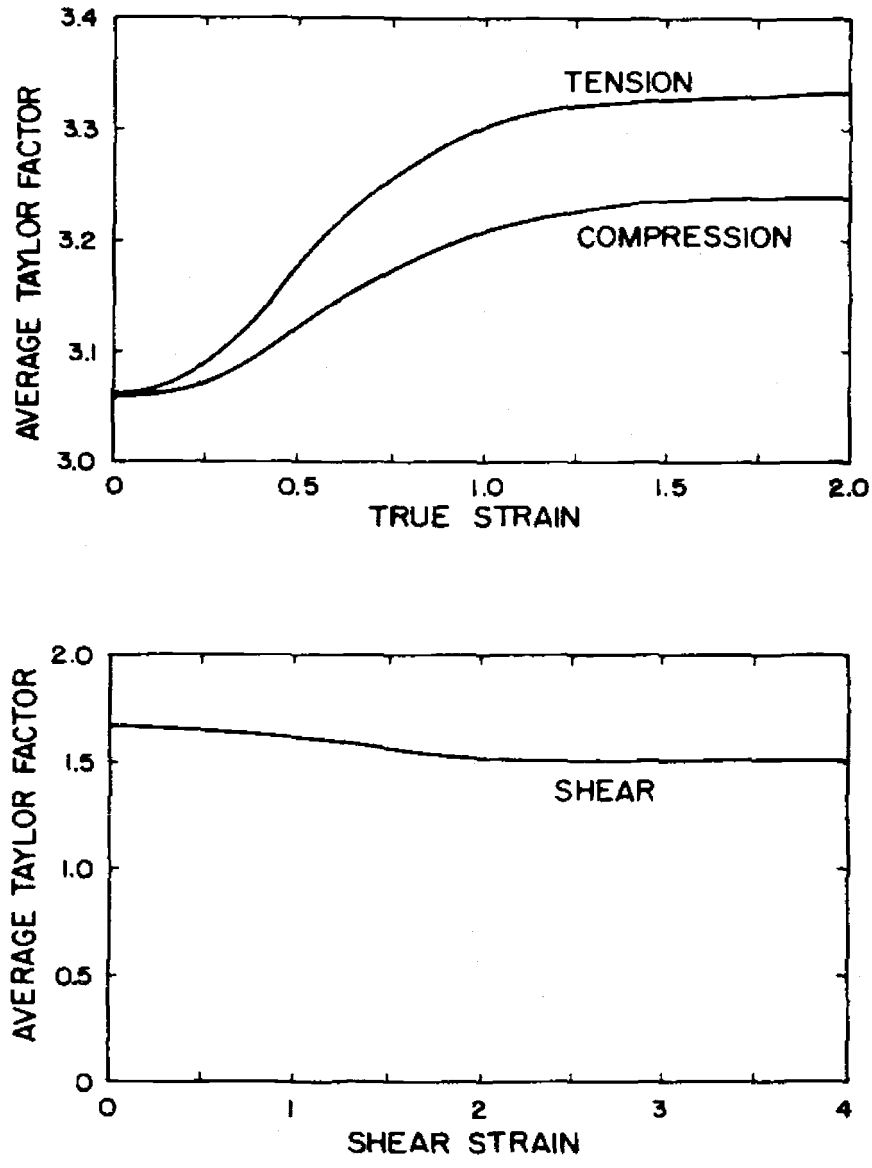

Figure 5.1: Calculations of the evolution of average Taylor factors with strain. (Top) Tension and compression. (Bottom) Shear [27].

6. EXPERIMENTAL PROCEDURE

The polycrystalline aluminum used in this investigation was provided as rod of 99.999% purity. The amounts of all the impurities are shown below:

Impurity	Amount in ppm	Impurity	Amount in ppm	Impurity	Amount in ppm
Ag	<0.01	Ga	<0.005	P	0.9
Au	<0.05	Ge	<0.01	Pd	<0.005
As	<0.005	H	0.15	S	<0.005
B	0.14	In	<0.005	Sb	<0.005
Be	<0.001	K	<0.05	Se	<0.03
C	<3.8	La	0.0017	Si	1.4
Ca	<0.01	Li	<0.001	Sn	<0.01
Ce	0.0024	Mg	0.23	Th	0.28 *
Cl	<0.01	Mn	0.06	Ti	0.04
Cr	0.17	Mo	<0.005	U	0.13 *
Cs	<0.005	N	<5	V	<0.01
Cu	<0.3	Na	<0.005	W	<0.005
F	<0.05	Ni	<0.005	Zn	0.17
Fe	0.18	O	<4.0	Zr	0.020

* The amount of impurity is in ppb.

The hollow torsion specimens were machined as in Figure 6.1. The outer diameter was 8.89 mm and the inner diameter was 4.445 mm. The gage length, L, was 2.54 mm. The specimens are shown in Figure 6.2. The specimens were annealed at 425°C for one hour in the annealing furnace, Figure 6.3. The tests were then performed on an Instron 8521 servohydraulic biaxial testing machine which is an all-digital system illustrated in Figure 6.4. A 500 in-lbs torque load cell was

used in the experiments. The experiments were done at high temperature, T = 371°C, using a resistance heat furnace. A thermocouple was used to measure the temperature at the surface of the specimens. The temperature of 371°C was hold for two hours before starting the tests, so there was no temperature gradient during the tests. The Control System consists of two basic units which provide all the digital control and indicating functions for the system. The first unit of the control system is the front panel console contains the operating controls, pushbuttons, indicators, and displays necessary to set up, run, and gather data for the material test. The second unit is the so-called "tower" console, which contains the microprocessors and transducer channel controller modules that form the heart of the control system. This is illustrated in Figure 6.5.

During the tests, a computer, that was connected to the system, was recording the time step in seconds, the axial position in inches, the load in lbs., the angle of twist (θ) in degrees, and the torque in in-lbs.

The torsion specimens slide freely within the grips in the axial direction just prior to deformation. However, substantial friction between the specimen ends and the slots of the machine grips develops after twisting the specimens, with the consequence that dimensional changes of the gauge section may result in axial stresses. This tendency, however, is mitigated by one of the machine grips being spring loaded so that it may undergo a 1 mm axial displacement with a stress of only 0.1 MPa. Since the dimensional changes are expected to be less than 0.04L [33], where L is the gage length, the stresses generated are not expected to dramatically affect the mechanical data (i.e. torque).

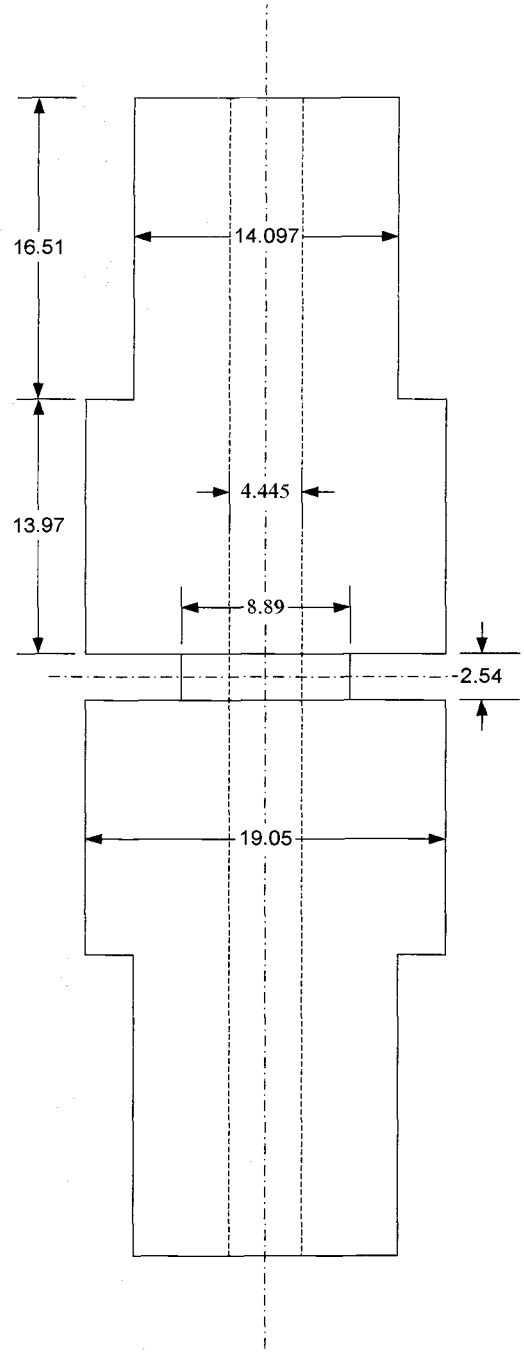

Figure 6.1: Dimensions of torsion specimens (all dimensions are in mm).

Figure 6.2: The hollow torsion specimens.

Figure 6.3: The annealing furnace.

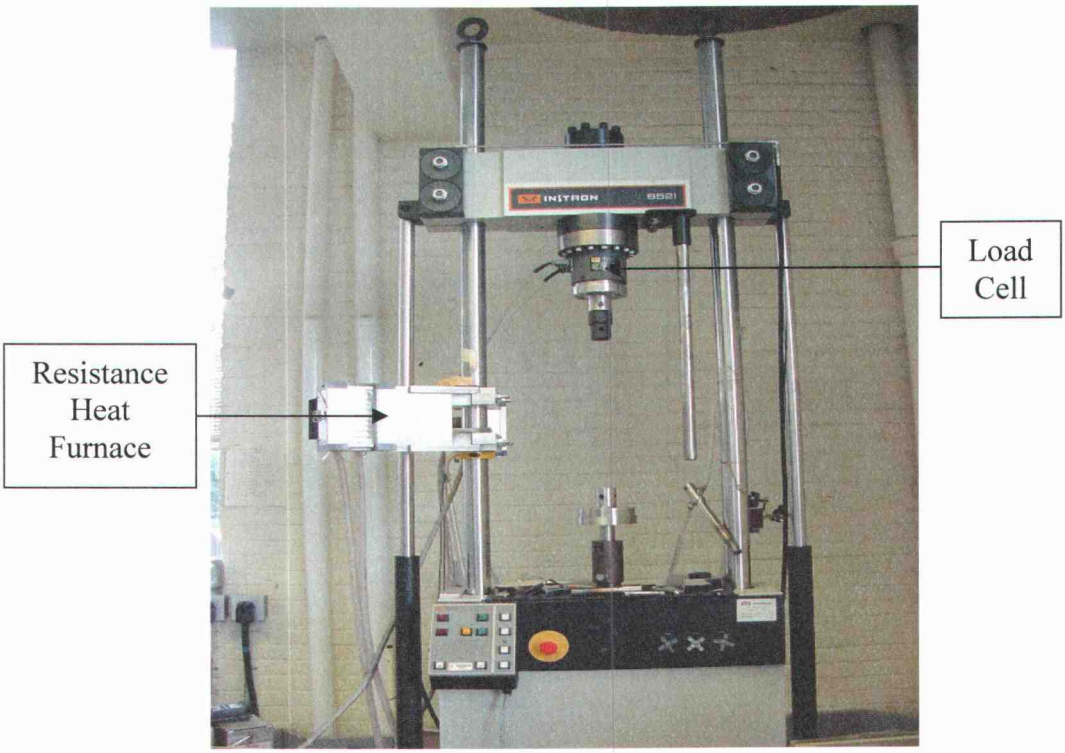

Figure 6.4: Instron 8521 servohydraulic biaxial testing machine with the resistance heat furnace.

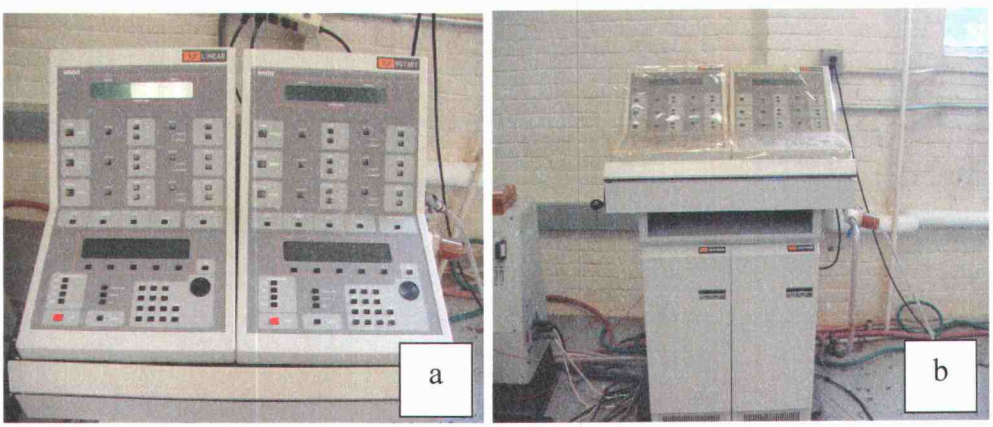

Figure 6.5: The Control System; (a) The front panel console, (b) The tower console.

Two samples were cut from one of the torsion specimens at 0° and 90° to the torsion axis. The samples were polished mechanically with the standard procedure then etched with the Poulton's reagent consisting of:

- 12 ml HCL conc.
- 6 ml HNO_3 conc.
- 1 ml HF (48%)
- 1 ml H_2O.

The microstructure was clearly visible with the naked eye, and was also observed under optical microscope. The photographs of the grain structure were taken by a digital camera mounted on a low magnification microscope. The mean grain size was calculated using the linear intercept method and found to be = 0.888 mm.

Shear stresses and strains at the outer radius were determined from the torque (M) and angle of twist (θ) measurements using the usual equations

$$\tau = \frac{3M}{2\pi\left(R^3 - r^3\right)} \tag{6.1}$$

$$\gamma_m = \frac{r_m\,\theta}{L} \tag{6.2}$$

where R is the specimen outer radius, r is the inner radius, r_m is the mean radius, and L is the gage length. τ is the shear stress, and γ_m is the mean shear strain. The shear stress and mean shear strain were converted to the equivalent-uniaxial stress and equivalent-uniaxial mean strain using the von Mises relation

$$\bar{\sigma} = \sqrt{3}\ \tau \tag{6.3}$$

$$\bar{\varepsilon}_m = \frac{\gamma_m}{\sqrt{3}} \tag{6.4}$$

Compression stresses and strains were determined from the load (F) and axial position difference (ΔL) measurements using the usual equations

$$\varepsilon = \frac{\Delta L}{L} \tag{6.5}$$

$$\sigma = \frac{F}{\pi (R^2 - r^2)} \tag{6.6}$$

Shear stresses and strains for solid torsion specimens were determined by Kassner in earlier tests, [18], using the equations, [34],

$$\bar{\sigma} = \frac{M}{2\pi R^3} (3 + n + m)\ \sqrt{3} \tag{6.7}$$

$$\bar{\varepsilon} = \frac{R\ \theta}{L\ \sqrt{3}} \tag{6.8}$$

where M is the applied torque, θ is the angle of twist, R is the specimen radius, and L is the gage length. The term n is the strain-hardening exponent (n = 0 at steady state), and the term m is the strain-rate sensitivity exponent (assumed = 0.225 for aluminum once steady state is achieved, i.e. $\bar{\varepsilon} \cong 0.2$). The strain-hardening and strain-rate sensitivity exponents are determined by $(\partial \ln M/\partial \ln \theta)_{T,\dot{\theta}}$ and $(\partial \ln M/\partial \ln \dot{\theta})_{T,\theta}$, respectively.

Compression specimens that were extracted from quenched solid specimens had a compression axis that was coincident with the original torsion axis and an aspect ratio (length/diameter) $\cong$ 1.0. Compression tests for the quenched specimens (ambient temperature tests) used a 0.20 plastic strain offset and a strain rate of 1.67 $\times$ 10^{-4} s^{-1}. The high temperature compression test of the hollow specimens used a 0.10 strain offset to mitigate any unanticipated compliance. The elevated-temperature compression tests were performed within 5 seconds of unloading from torsion. An advantage of the hollow specimens is that there is less of a strain gradient than solid specimens and this may lead to more accurate stress measurements. Frictional effects were not considered.

7. RESULTS AND DISCUSSION

Figure 7.1(a) illustrates the observed equivalent uniaxial stress, $\bar{\sigma}$, versus equivalent uniaxial strain, $\bar{\varepsilon}$, of Al deformed in torsion at 371°C at an equivalent uniaxial strain-rate of 5.04×10^{-4} s^{-1}.

Procedures to assess any texture softening are combinations of the following mechanical tests reported by Kassner earlier [35], but are re-evaluated now, (1) and (2), and the recent hollowed specimens tests, (3),:

(1) T-Q-T tests in which specimens are torsionally deformed at elevated temperature to various strains within the softening regime, quenched to preserve the microstructure, and then torsionally deformed (coincident with the elevated-temperature straining) to plastic yield at ambient temperature.

(2) T-Q-C tests in which specimens undergo elevated-temperature torsion deformation, followed by a quench, sectioning, and ambient-temperature compression tests in which the compression axis is coincident with the elevated- temperature torsion axis. The plane of maximum resolved shear stress changes from 90° to the torsion axis to 45° to the axis.

(3) T-HT-C tests in which hollowed torsion specimens undergo elevated temperature deformation followed (without sectioning, of course) by elevated temperature compression. Tests are similar to (2) but with a smaller strain gradient and compression deformation at the same temperature as torsion tests. In (2), the compression specimens are cut and machined from the torsion specimens, but with procedure (3), this step is avoided by using a relatively short gage length.

If the softening is due principally to texture or microstructure effects, then the ambient-temperature torsion tests that follows the elevated-temperature tests should show a reduction in yield stress with increasing elevated-temperature pre-strain within the softening regime. Figure 7.1(b) shows the results of 8 procedure (1) T-Q-T tests. Some scatter is present of uncertain origin, perhaps non-uniform quenching. With elevated temperature pre-strain the ambient-temperature yield stress decreases by roughly 15-20%, as expected. If the softening is due to a change in mechanism (e.g., GBS, Coble creep, etc.), then the ambient temperature decrease in yield stress with pre-strain would not be expected to be observed. This is because these mechanisms are expected to disappear at ambient temperature.

The T-Q-C tests are reported in Figure 7.1(c). Fourteen compression specimens were extracted from five torsion specimens tested to various elevated-temperature strains. Interestingly, the data show a trend of increasing ambient-temperature compressive yield strength with increasing elevated temperature pre-strain in the softening regime. The increase is about 10%, although some scatter is present, again, of uncertain origin. If the elevated temperature softening is due to a change in microstructure, then the ambient temperature compression tests should show a decrease rather than an increase in strength with elevated-temperature pre-strain. The observed trends are, perhaps, most easily explained by the development of a texture at elevated temperature.

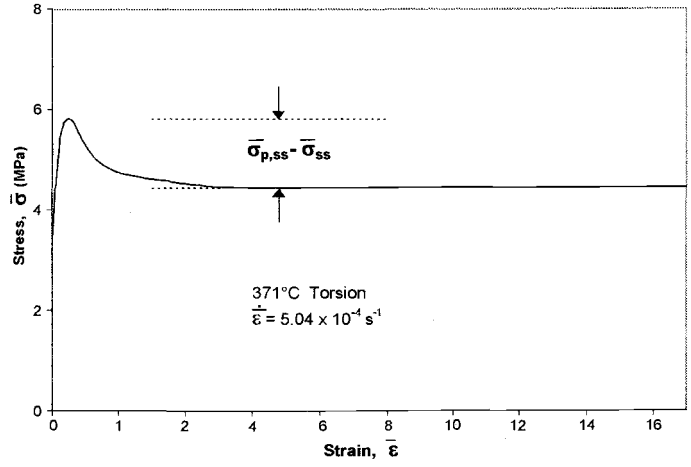

Figure 7.1(a): The equivalent uniaxial stress versus equivalent uniaxial strain of solid specimens of Al deformed in torsion at 371°C.

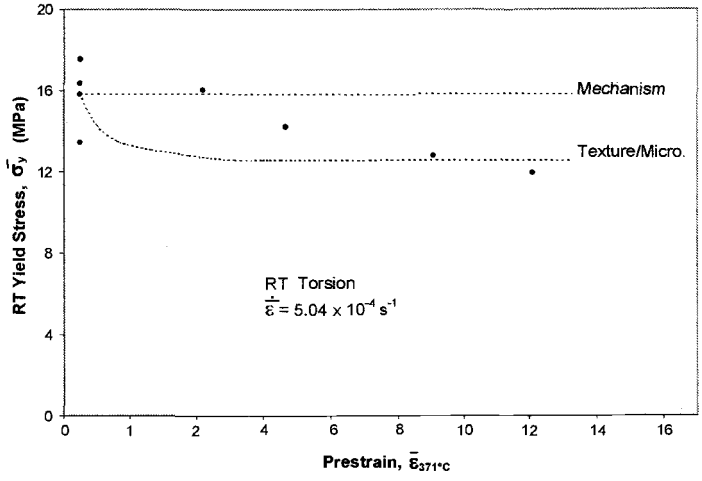

Figure 7.1(b): The ambient temperature torsional yield stress of Al pre-deformed to various strains in torsion at 371°C. The ambient temperature yield stress decreases coincidentally with elevated-temperature prestrain indicating a change in deformation mechanism is not responsible for the elevated-temperature shear softening.

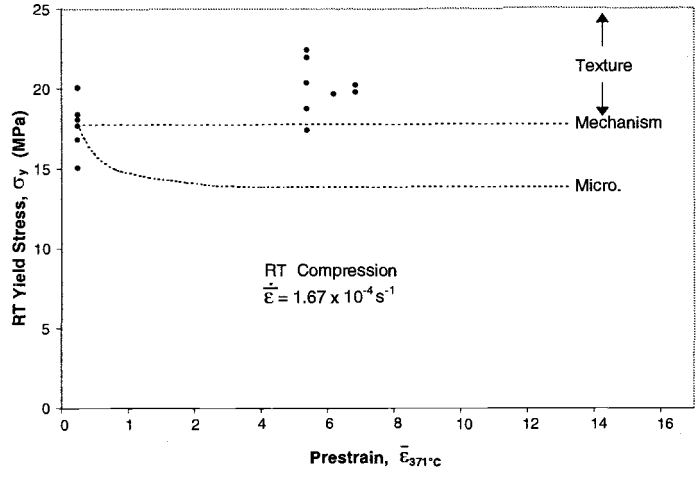

Figure 7.1(c): The ambient temperature compression yield stress of solid Al predeformed to various strains in torsion at 371°C. The compression axis is coincident to the prior torsion axis. The slight increase in yield stress with elevated-temperature suggests that essentially all of the elevated-temperature shear stress reduction is due to a decrease in the Taylor factor.

Figure 7.2 illustrates the (~ 16%) softening of a hollow torsion specimen to a strain of about 1.3. The behavior is quite similar to that of the solid specimens. The elevated temperature torsion tests consisted of deformation to various strains within the softening regime. The tests were terminated at four strain levels, the peak strain of about 0.25, the strain of about 0.45, the strain of about 0.69, and the nearly fully softened state, at a strain of about 1.2. Upon termination of the tests, specimens were quickly unloaded and compressed. The elevated temperature compressive stress increases with torsion pre-strain in the softened regime. The increase is slightly less than that of the unhollowed ambient-temperature compression tests. This difference may be a consequence of the unhollowed region of solid specimens experiencing greater hardening in the "interior" portions of the compression specimen at the larger strains as compared to that at the peak stress.

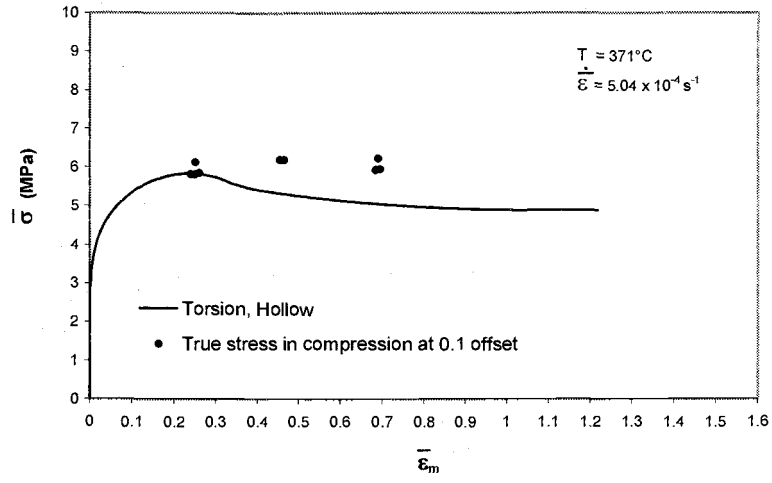

(a)

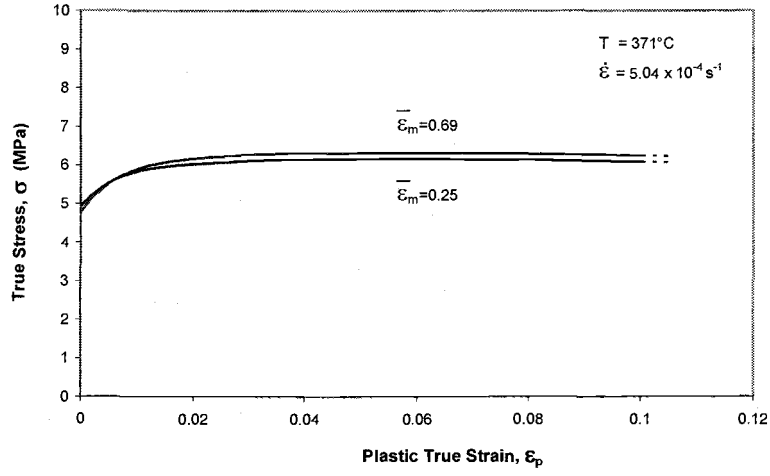

(b)

Figure 7.2: (a) The 371°C equivalent uniaxial stress versus equivalent uniaxial strain of hollow torsion specimens and the corresponding compressive yield stress (0.10 strain offset) at the same strain rate and temperature subsequent to various (pre)strains in torsion. Again, the slight increase in strength suggests that the shear stress decrease is due to decreases in the Taylor factor. **(b)** The stress versus strain behavior of two compression tests with different torsion prestrains.

Figures 7.3 and 7.4 illustrate the microstructures of the hollowed torsion specimens after annealing at 425°C for one hour at planes parallel and perpendicular to the torsion axis under the optical microscope. The mean grain size is 0.888 mm.

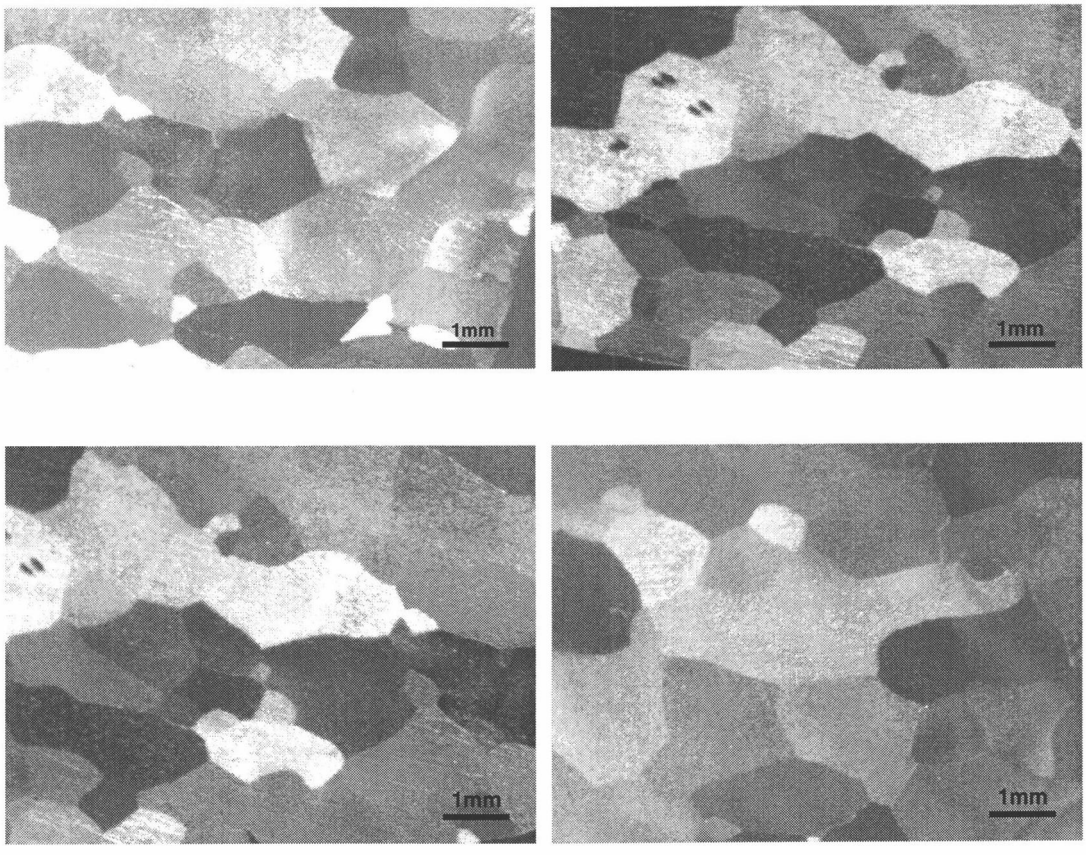

Figure 7.3: The microstructures of the hollowed torsion specimens after annealing at 425°C for one hour at a plane parallel to the torsion axis under the optical microscope.

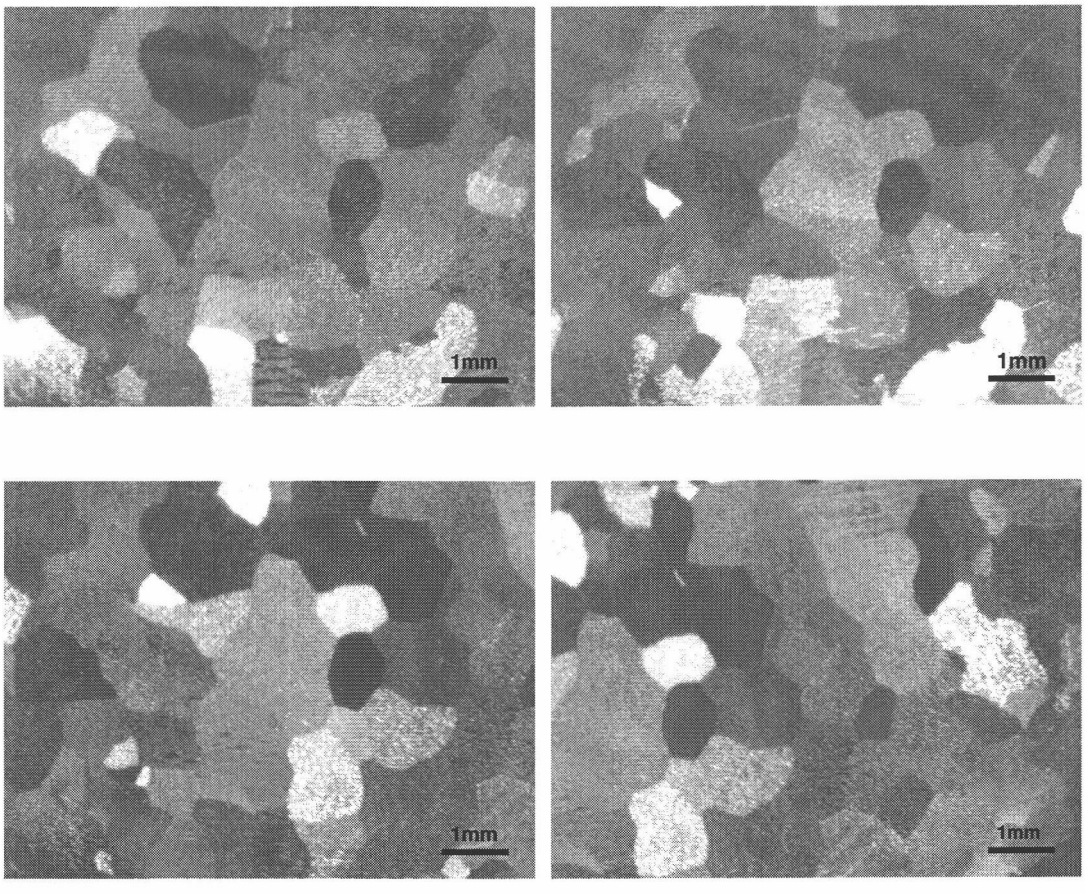

Figure 7.4: The microstructures of the hollowed torsion specimens after annealing at 425°C for one hour at a plane perpendicular to the torsion axis under the optical microscope.

If the "softened" regime specimens are compressed along the torsion axis, the average Taylor factor for A^2, C, and B^1 textures (calculated with the aid of [36]) would be 3.06. If just B^1 is used, a Taylor factor of about 3.1 is obtained (C is associated with a fairly low factor of about 2.5). Thus, based on the observed textures in pure aluminum, we expect about the same value of Taylor factor for the compression tests on the prior-torsionally deformed specimens as for a random array of polycrystals deformed in compression. Therefore, based on this procedure,

the ambient temperature compressive flow stress is not expected to decrease if all three textures are equally present or if the B^1 texture dominates. Therefore, the experimental results appear basically consistent with the predictions of a texture explanation for elevated temperature softening. Interestingly, they are also indirectly supportive of a dominating B^1 texture rather than an additional C component for pure aluminum. Also, the aluminum single crystal experiments in which the torsion axis was coincident with the soft [111], only hardening is observed at elevated temperature, as would be expected according to the texture explanation. [Compression stresses are slightly higher than the peak torsion stresses. This may be partly due to (unaccounted) constraint in compression.]

8. CONCLUSIONS

Pure aluminum deformed to elevated temperature in pure shear (torsion) reaches a broad "peak" stress and then undergoes about a 17% decrease in flow stress with deformation to roughly 1-2 equivalent uniaxial strain. Beyond this strain the flow stress is approximately constant. Experiments were performed where specimens were deformed in torsion to various strains within the softening regime followed by compression tests at ambient and elevated temperature. Analysis of the compressive yield strengths indicate that the softening is substantially explained by a decrease in the average Taylor factor during elevated temperature deformation in pure shear.

BIBLIOGRAPHY

1. S.P. Belyayev, V.A. Likhachev, M.M. Myshlyaev and O. N. Senkov, "Dynamic Recrystallization of Aluminum," Phys. Met. Metall., 52 (1981), 143-152.

2. V.A. Likhachev, M.M. Myshlyaev, O.N. Senkov and S.P. Belyayev, "Creep of Aluminum in Torsion under Superplasticity Conditions," Phys. Met. Metall., 52 (1981), 156-164.

3. V.A. Likhachev, M.M. Myshlyaev and O.N. Senkov, "Laws of Superplastic Behavior of Al in Torsion" (Inst. of Solid State Physics, Chernogolovka, Russia, 1981), (in Russian).

4. M.M. Myshlyaev, O.N. Senkov and V.A. Likhachev, "Regularities of Mechanical Behavior and Evolution of Structure of Aluminum and its Alloys Under Superplasticity," Strength of Metals and Alloys, ed. H.J. McQueen et al. (Oxford: Pergamon, 1985), 841-846.

5. C. Perdrix, M.Y. Perrin and F. Montheillet, "Mechanical Behavior and Structural Change of Aluminum During Large-Amplitude Hot Deformation," Mem. Et. Sci. Rev. Metal., 78 (1981), 309-320.

6. S. Gourdet, E. Konopleva, H.J. McQueen and T. Montheillet, "Recrystallization During Hot Deformation of Aluminum" (Paper presented at the Fifth International Conference on Aluminum Alloys, Grenoble, France, 1996, Mater. Sci. Forum), 217-222, 441-446.

7. S. Gourdet and T. Montheillet, "An Experimental Study of the Recrystallization Mechanism During Hot Deformation of Aluminum," Mater. Sci and Eng., A283 (2000), 274-288.

8. H.J. McQueen, O. Knustad, N. Ryum and J.K. Solberg, "Microstructural Evolution in Al Deformed to Stains of 60 at 400°C," Scripta Metall., 9 (1985), 73-78.

9. J.K. Solberg, H.J. McQueen, N. Ryum and E. Nes, "Influence of Ultra-High Strains at Elevated Temperatures on the Microstructure of Aluminum. Part I," Phil. Mag., 60A (1989), 473-485.

10. H.J. McQueen, E. Evangelista and M.E. Kassner, "The Classification and Determination of Restoration Mechanisms in the Hot Working of Al Alloys," Z. Metall., 82 (1991), 336-345.

11. H.J. McQueen and W. Blum, "Dynamic Recovery: Sufficient Mechanism in the Hot Deformation of Al (<99.99)," Mater. Sci. and Eng., Vol A290 (2000), 95-107.

12. H.J. McQueen, "Textures in Dynamic Recovery and Recrystallization" (Paper presented at ICOTOM 12, ed. J.A. Spunar, Ottawa: NRC Research Pub., 1999), 836-841.

13. T. Pettersen, "A Study of the Deformation and Recrystallization Microstructures and Textures in AA6060 and AA 6082 Alloys" (Ph.D. thesis, Norwegian Univ. Sci. and Tech., Trondheim, Norway, 1999).

14. T. Pettersen and E. Nes, Materials Science Forum, Vol 331-337 (2002), 601.

15. M.E. Kassner, "Large Strain Deformation of Aluminum Single Crystal: A Critical Test for Geometric Dynamic Recrystallization," Metall. Trans., 20A (1989), 2182-2185.

16. M.E. Kassner and M.E. McMahon, "The Dislocation Microstructure of Aluminum Deformed to Very Large Steady State Creep Strains," Metall. Trans., 18A (1987), 835-846.

17. M.E. Kassner, M.M. Myshlyaev, and H.J. McQueen, "Large Strain Torsional Deformation of Aluminum at Elevated Temperatures," Mater. Sci. and Eng., 108A (1989), 45-61.

18. M.E. Kassner, N.Q. Nguyen, G.A. Henshall, and H.J. McQueen, "The Effects of Temperature and Strain Rate on the Extended Ductility of Aluminum," Mater. Sci. and Eng., A132 (1991), 97-105.

19. M.E. Kassner, "Large Strain Deformation of Aluminum Single Crystals at Elevated Temperature," Hot Deformation of Aluminum Alloys II, ed. T.R. Bieler, L.A. Lalli, and S.P. McEwen (Warrendale: TMS, 1998), 3-8.

20. D.A. Hughes, M.E. Kassner, M.G. Stout and J.S. Vetrano, "Metal Forming at the Center for Excellence for the Synthesis and Processing of Advanced Materials," J. Metals, 50 (1998), 16-22.

21. M.E. Kassner and M.-T. Perez-Prado, "Five Power-Law Creep in Single Phase Metals and Alloys," Prog. Mater. Sci., 45 (2000), 1-102.

22. S.C. Shrivastava, J.J. Jonas, and G.R. Canova, "Equivalent Strain in Large Deformation Torsion Testing: Theoretical and Practical Considerations," J. Mech. Phys. Solids, 30 (1982), 75-90.

23. R.D. Doherty, D.A. Hughes, F.J. Humphreys, J.J. Jonas, D. Juul Jensen, M.E. Kassner, W.E. King, T.R. McNelley, H.J. McQueen, A.D. Rollett, "Current Issues in Recrystallization: a Review," Materials Science and Engineering, A238 (1997), 219-274.

24. M.E. Kassner, "Creep," to be published.

25. S. Barabes, C. Daraio, M.E. Kassner, T.A. Hayes, M.Z. Wang, to be published.

26. B.D. Cullity, Elements of X-Ray Diffraction, 2nd ed. (Reading, Mass.: Addison-Wesley, 1978).

27. G. Krauss, "Deformation, Processing, and Structure" (Papers presented at the 1982 ASM Materials Science Seminar, St. Louis, Missouri), 1984, 1-46.

28. G.I. Taylor, "Plastic Strain in Metals," J. Inst. Metals, Vol 62, 1938, 307-324.

29. J. Gil-Sevillano, P. van Houtte and E. Aernoudt, "Large Strain Work Hardening Textures," Prog. Mater. Sci., Vol 25, 1980, 69-412.

30. U.F. Kocks, "The Relation Between Polycrystal Deformation and Single Crystal Deformation," Met. Trans., Vol 1, 1970, 1121-1143.

31. G.Y. Chin, "The Role of Preferred Orientation in Plastic Deformation," in Inhomogeneity of Plastic Deformation, edited by R.E. Reed-Hill, American Society for Metals, 1973, 83-112.

32. J.F.W. Bishop and R. Hill, "A Theory of the Plastic Distortion of a Polycrystalline Aggregate Under Combined Stresses," Phil. Mag., Vol 42, 1951, 414-427.

33. R. Horiuchi, J. Kaneko, A.B. Elsebai and M.M. Sultan, "The characteristics of the Hot Torsion Test for Assessing Hot Workability of Aluminum Alloys," Institute of Space and Aeronautical Science, University of Tokyo, Rep. 443, February 1970.

34. W.J. McGregor Tegart, Elements of Mechanical Metallurgy (New York: Macmillan, 1966).

35. M.E. Kassner and J.J. Oldani, "Large Strain Softening of Aluminum at Elevated Temperature" (Paper presented at the Ninth Inter-American Conference of Materials Technology, Univ. Chile, eds. Santiago, Chile: Editorial Universitaria, 1987), 219-223.

36. G.Y. Chin and W.L. Mammel, "Computer Solutions of the Taylor Analysis for Axisymmetric Flow," Trans. AIME, 239 (1967), 1400-1405.

APPENDIX

APPENDIX: Stress - Strain Curves

Equivalent-uniaxial stress versus equivalent-uniaxial mean strain and compression stress versus strain for the samples torsionally deformed at a temperature of 371°C at an equivalent uniaxial strain-rate of 5.04×10^{-4} s^{-1}.

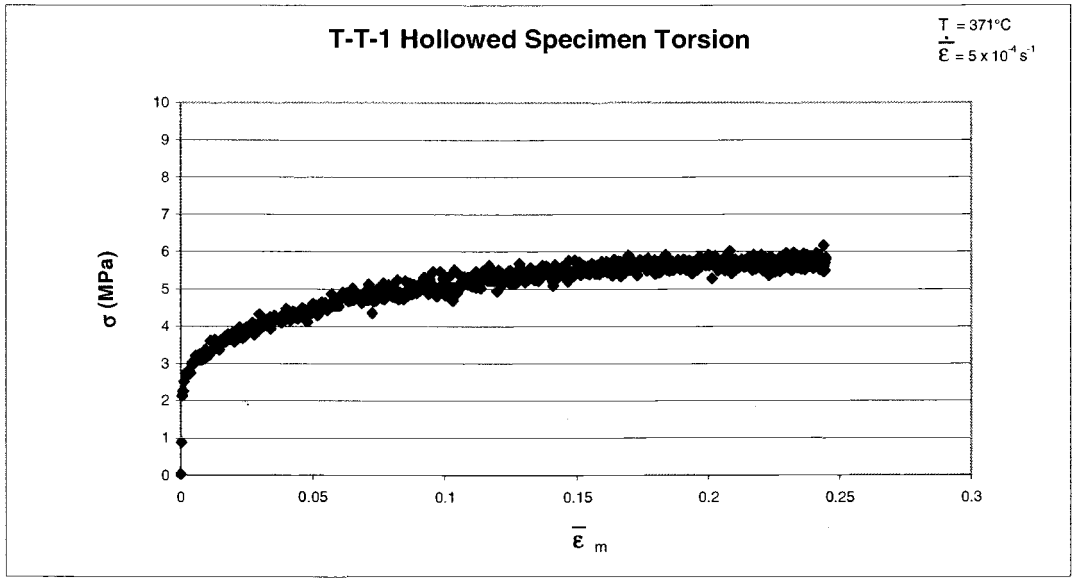

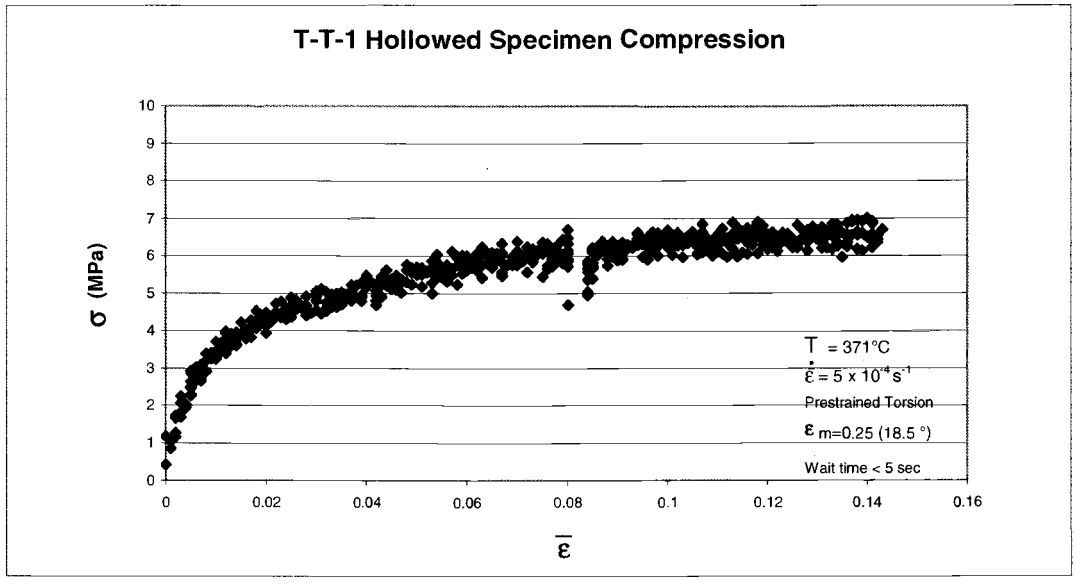

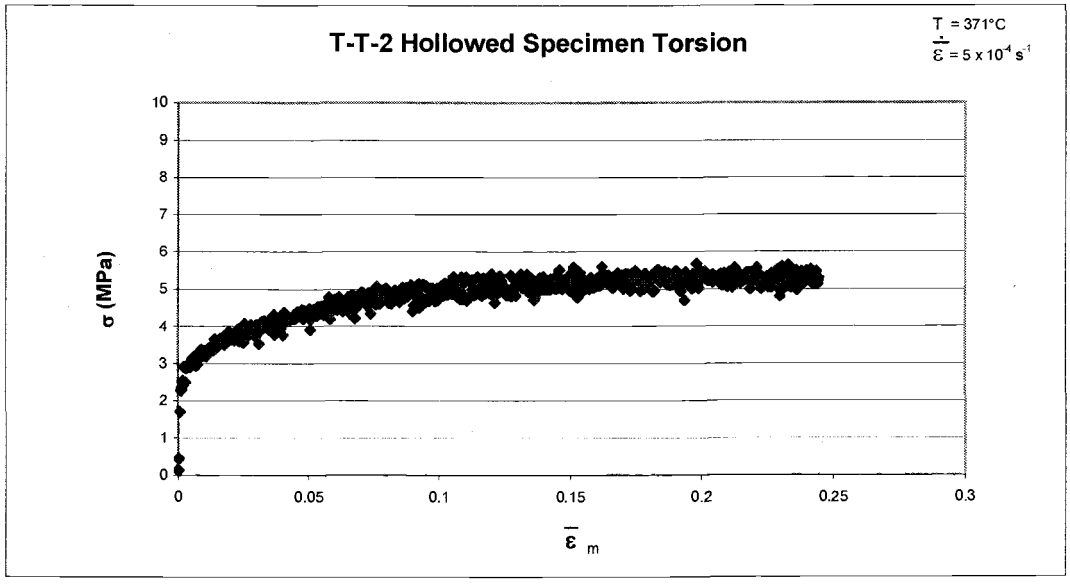
T-T-2 Hollowed Specimen Torsion
T = 371°C
$\dot{\bar{\varepsilon}} = 5 \times 10^{-4}\ s^{-1}$
σ (MPa)
0
1
2
3
4
5
6
7
8
9
10
0
0.05
0.1
0.15
0.2
0.25
0.3
$\bar{\varepsilon}_m$

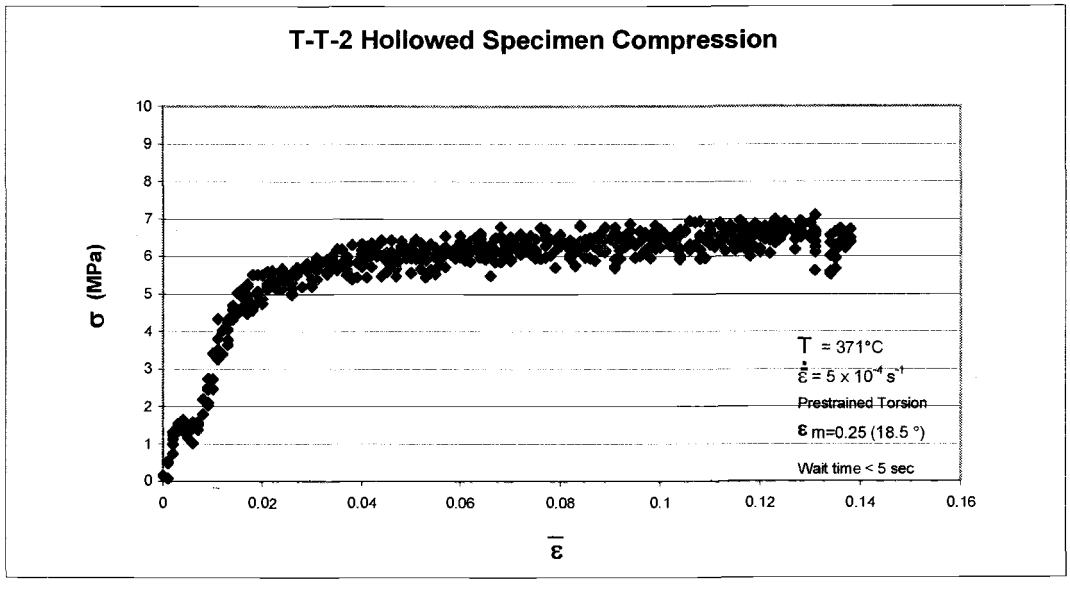
T-T-2 Hollowed Specimen Compression
σ (MPa)
0
1
2
3
4
5
6
7
8
9
10
0
0.02
0.04
0.06
0.08
0.1
0.12
0.14
0.16
$\bar{\varepsilon}$
T = 371°C
$\dot{\bar{\varepsilon}} = 5 \times 10^{-4}\ s^{-1}$
Prestrained Torsion
ε m=0.25 (18.5 °)
Wait time < 5 sec

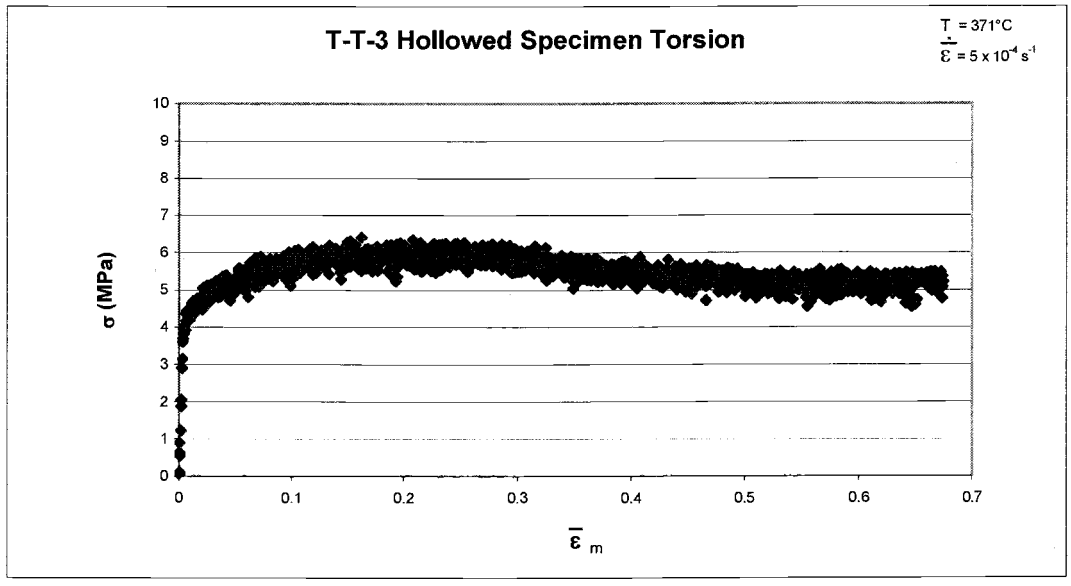
T-T-3 Hollowed Specimen Torsion
T = 371°C
$\dot{\bar{\varepsilon}} = 5 \times 10^{-4}\ s^{-1}$
σ (MPa)
$\bar{\varepsilon}_m$
0
1
2
3
4
5
6
7
8
9
10
0
0.1
0.2
0.3
0.4
0.5
0.6
0.7

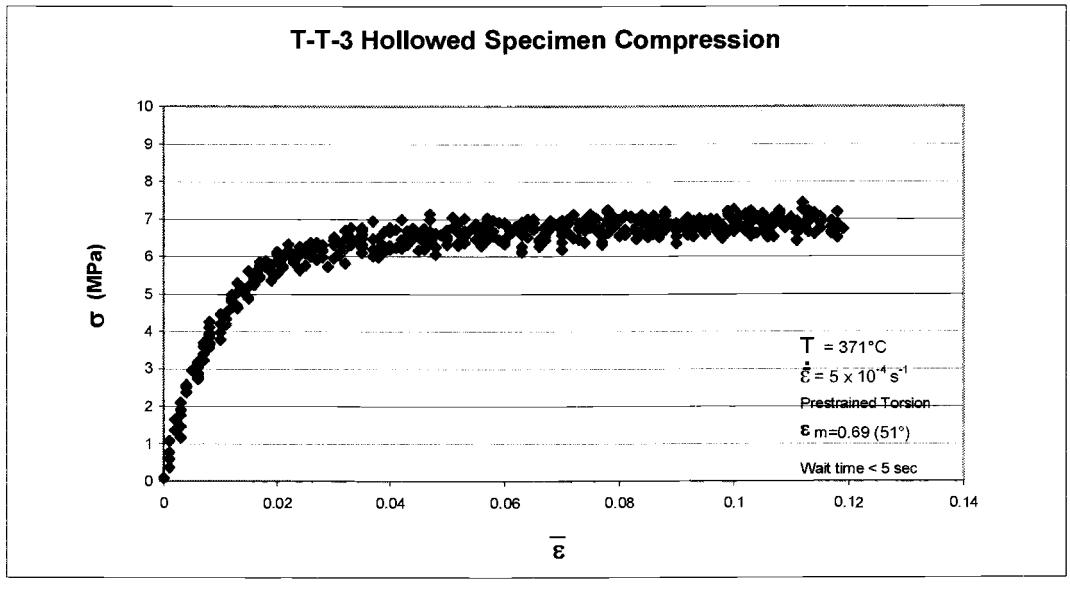
T-T-3 Hollowed Specimen Compression
σ (MPa)
$\bar{\varepsilon}$
T = 371°C
$\dot{\bar{\varepsilon}} = 5 \times 10^{-4}\ s^{-1}$
Prestrained Torsion
ε_m=0.69 (51°)
Wait time < 5 sec
0
1
2
3
4
5
6
7
8
9
10
0
0.02
0.04
0.06
0.08
0.1
0.12
0.14

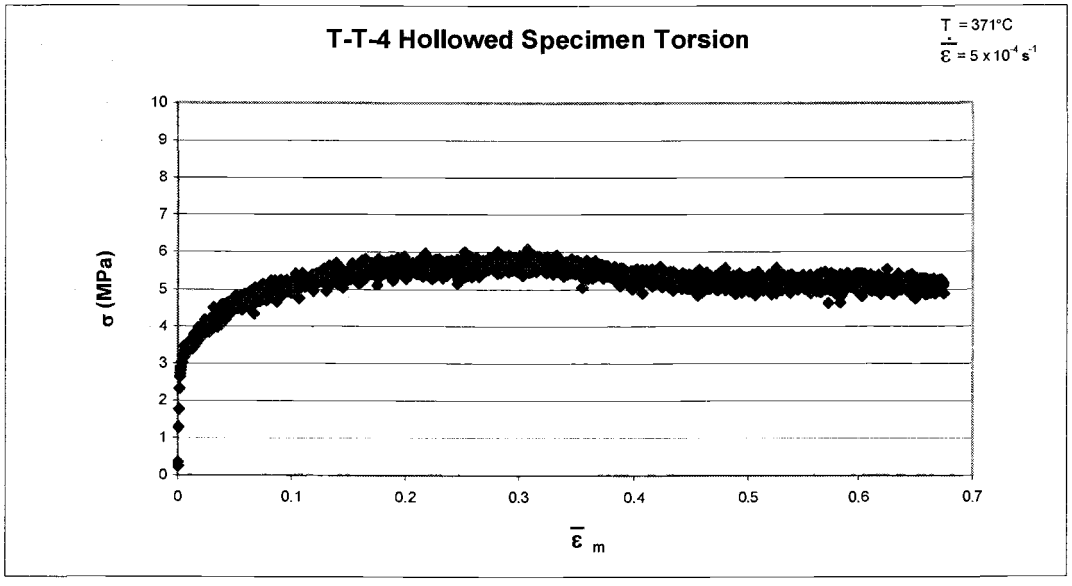
T-T-4 Hollowed Specimen Torsion
T = 371°C
$\dot{\bar{\varepsilon}} = 5 \times 10^{-4}\ s^{-1}$
σ (MPa)
$\bar{\varepsilon}_m$
0
1
2
3
4
5
6
7
8
9
10
0
0.1
0.2
0.3
0.4
0.5
0.6
0.7

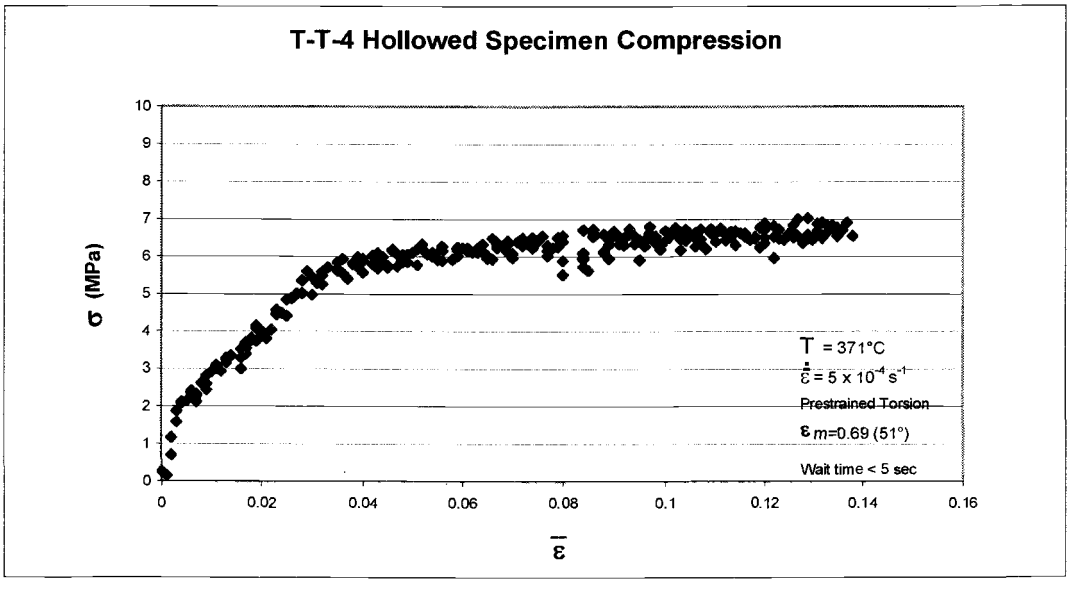
T-T-4 Hollowed Specimen Compression
σ (MPa)
$\bar{\varepsilon}$
T = 371°C
$\dot{\bar{\varepsilon}} = 5 \times 10^{-4}\ s^{-1}$
Prestrained Torsion
ε_m=0.69 (51°)
Wait time < 5 sec
0
1
2
3
4
5
6
7
8
9
10
0
0.02
0.04
0.06
0.08
0.1
0.12
0.14
0.16

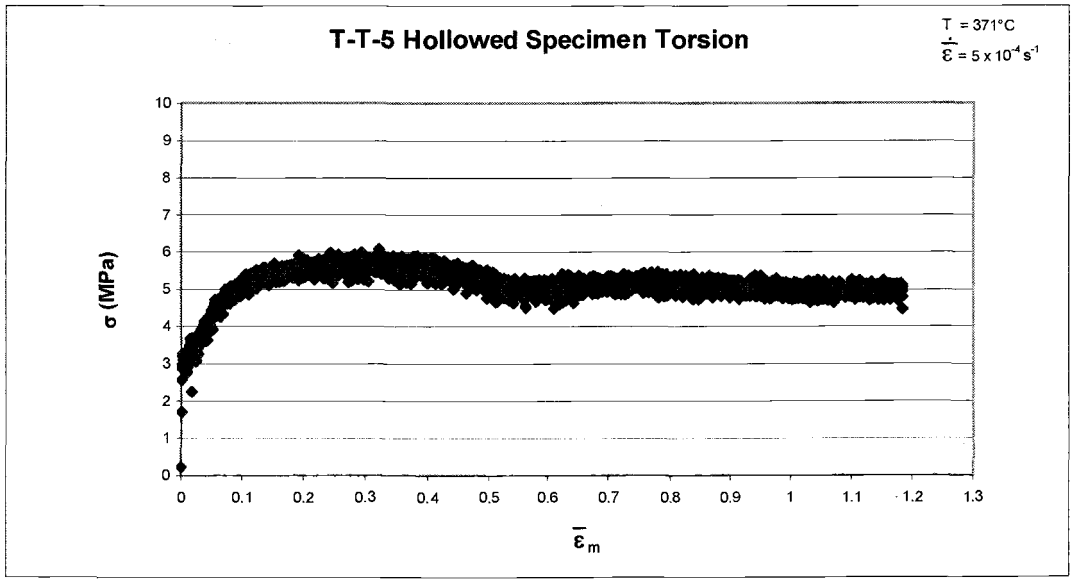
T-T-5 Hollowed Specimen Torsion
T = 371°C
$\dot{\bar{\varepsilon}} = 5 \times 10^{-4} s^{-1}$
σ (MPa)
$\bar{\varepsilon}_m$

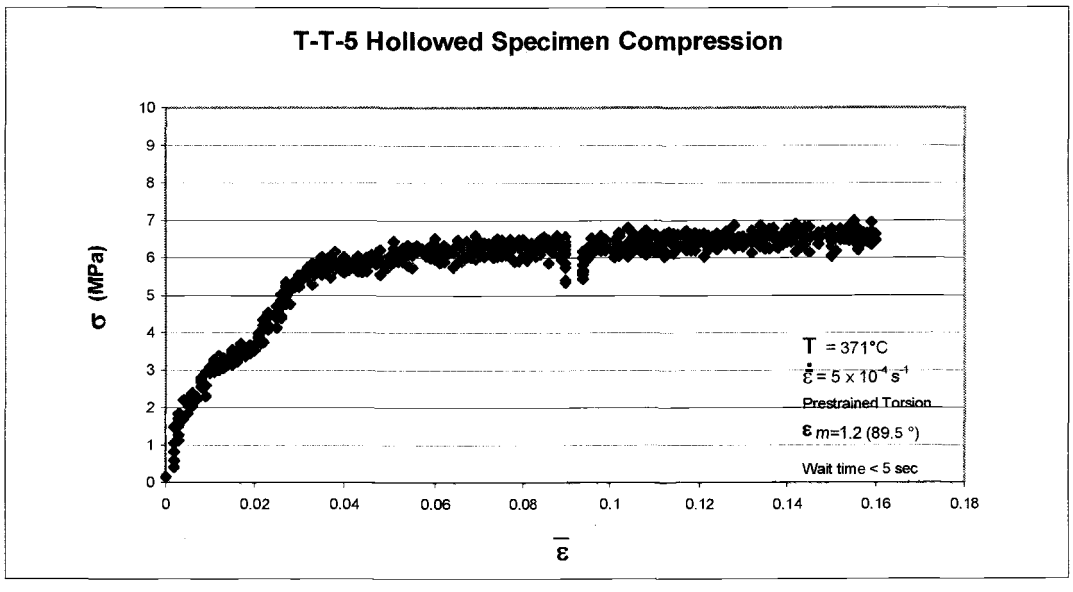
T-T-5 Hollowed Specimen Compression
σ (MPa)
T = 371°C
$\dot{\bar{\varepsilon}} = 5 \times 10^{-4} s^{-1}$
Prestrained Torsion
ε_m=1.2 (89.5 °)
Wait time < 5 sec
$\bar{\varepsilon}$

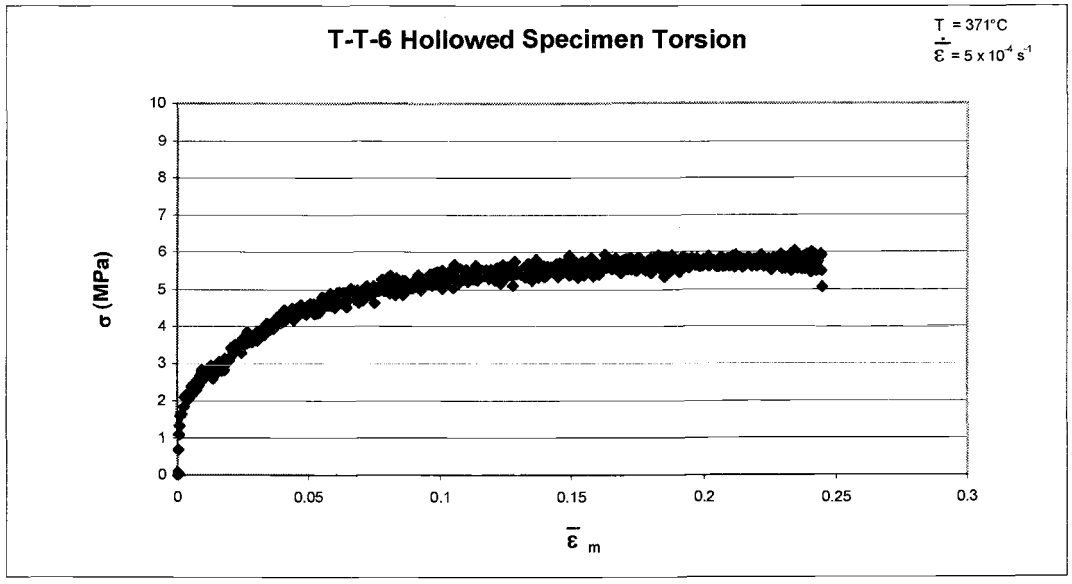
T-T-6 Hollowed Specimen Torsion
T = 371°C
$\dot{\bar{\varepsilon}} = 5 \times 10^{-4}\ s^{-1}$
σ (MPa)
$\bar{\varepsilon}_m$
0
1
2
3
4
5
6
7
8
9
10
0
0.05
0.1
0.15
0.2
0.25
0.3

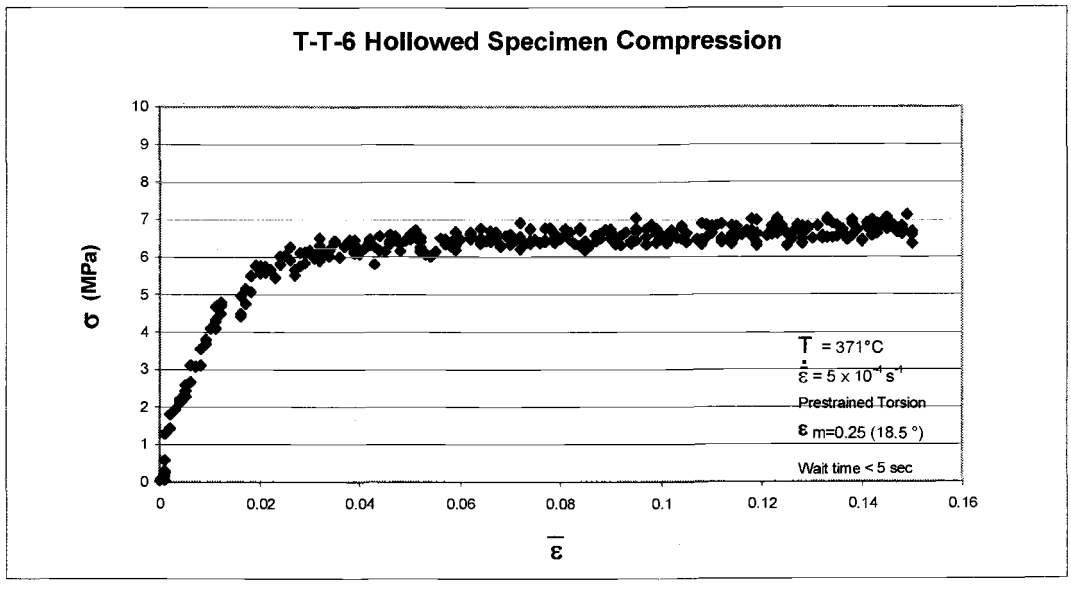
T-T-6 Hollowed Specimen Compression
σ (MPa)
$\bar{\varepsilon}$
T = 371°C
$\dot{\bar{\varepsilon}} = 5 \times 10^{-4}\ s^{-1}$
Prestrained Torsion
ε_m=0.25 (18.5 °)
Wait time < 5 sec
0
1
2
3
4
5
6
7
8
9
10
0
0.02
0.04
0.06
0.08
0.1
0.12
0.14
0.16

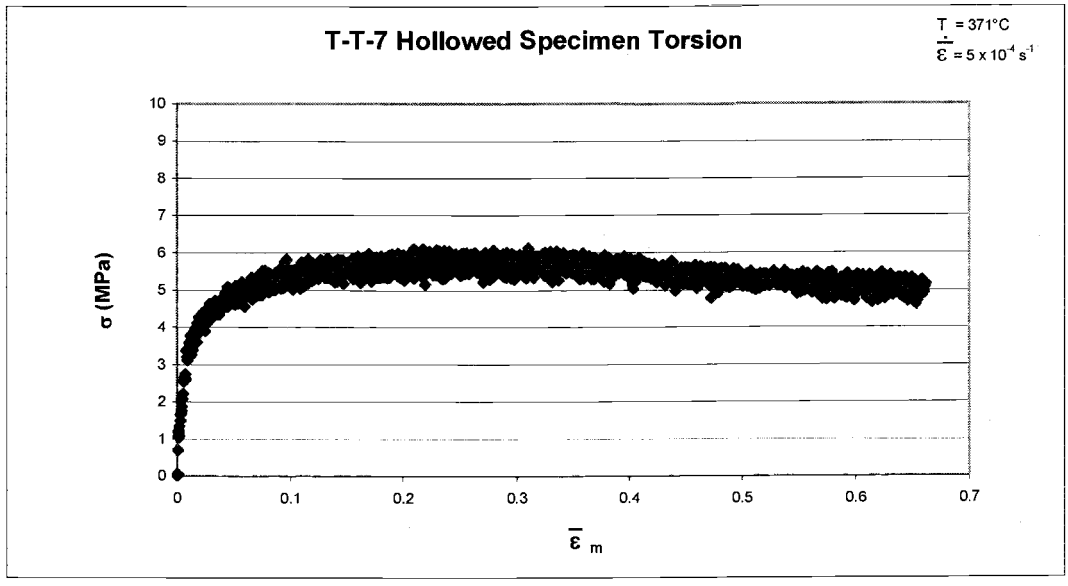
T-T-7 Hollowed Specimen Torsion
T = 371°C
$\dot{\bar{\varepsilon}} = 5 \times 10^{-4}\ s^{-1}$
σ (MPa)
$\bar{\varepsilon}_m$
0
1
2
3
4
5
6
7
8
9
10
0
0.1
0.2
0.3
0.4
0.5
0.6
0.7

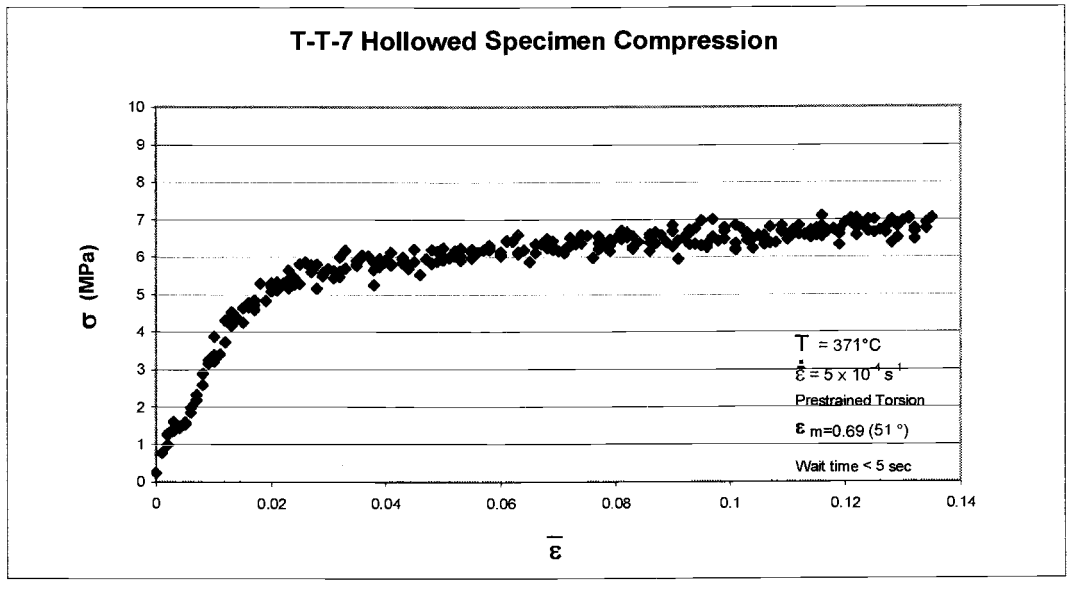
T-T-7 Hollowed Specimen Compression
σ (MPa)
$\bar{\varepsilon}$
T = 371°C
$\dot{\bar{\varepsilon}} = 5 \times 10^{-4}\ s^{-1}$
Prestrained Torsion
ε_m=0.69 (51 °)
Wait time < 5 sec
0
1
2
3
4
5
6
7
8
9
10
0
0.02
0.04
0.06
0.08
0.1
0.12
0.14

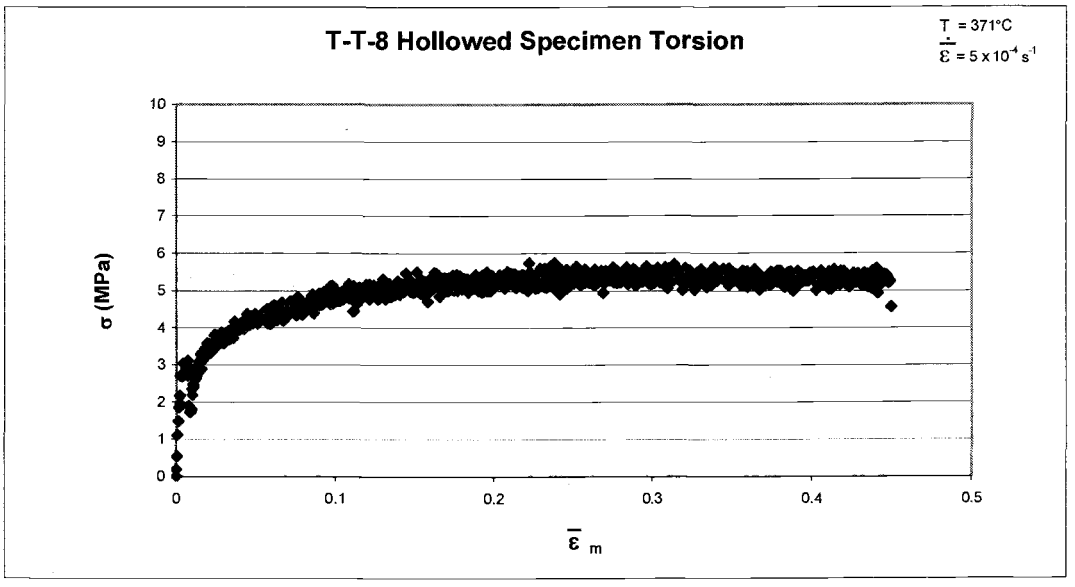
T-T-8 Hollowed Specimen Torsion
T = 371°C
$\dot{\bar{\varepsilon}} = 5 \times 10^{-4}\ s^{-1}$
σ (MPa)
$\bar{\varepsilon}_m$
0
1
2
3
4
5
6
7
8
9
10
0
0.1
0.2
0.3
0.4
0.5

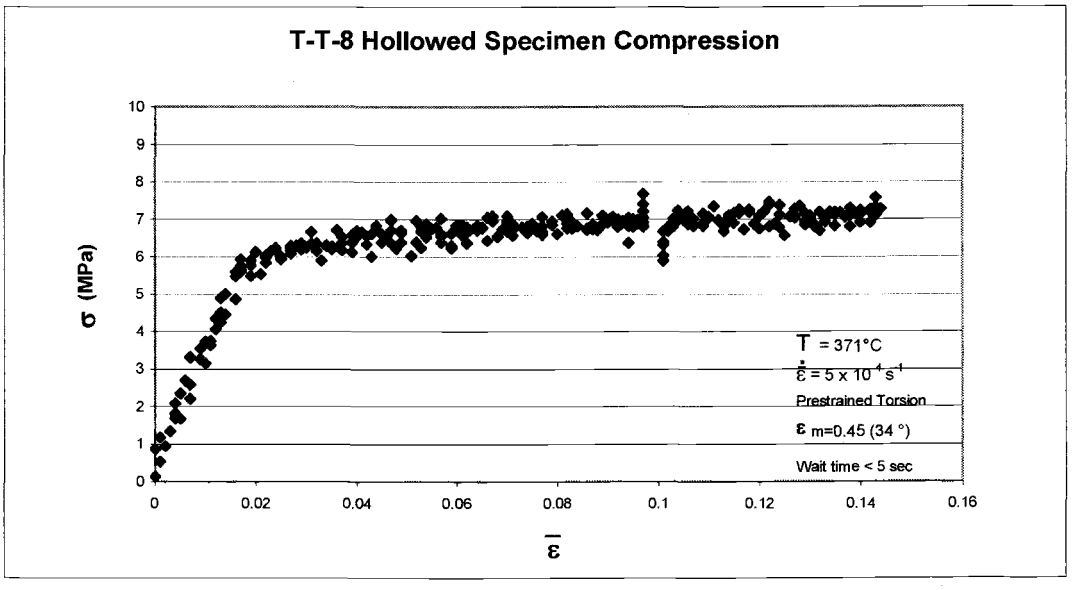
T-T-8 Hollowed Specimen Compression
σ (MPa)
$\bar{\varepsilon}$
T = 371°C
$\dot{\bar{\varepsilon}} = 5 \times 10^{-4}\ s^{-1}$
Prestrained Torsion
ε_m=0.45 (34 °)
Wait time < 5 sec
0
1
2
3
4
5
6
7
8
9
10
0
0.02
0.04
0.06
0.08
0.1
0.12
0.14
0.16

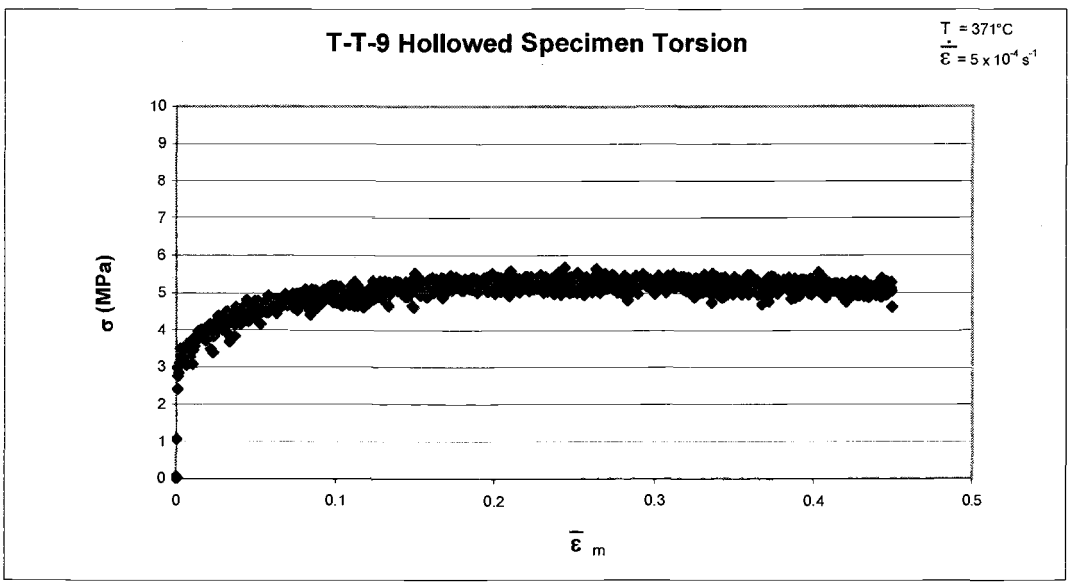
T-T-9 Hollowed Specimen Torsion
T = 371°C
$\dot{\bar{\varepsilon}} = 5 \times 10^{-4}\ s^{-1}$
σ (MPa)
$\bar{\varepsilon}_m$
0
1
2
3
4
5
6
7
8
9
10
0
0.1
0.2
0.3
0.4
0.5

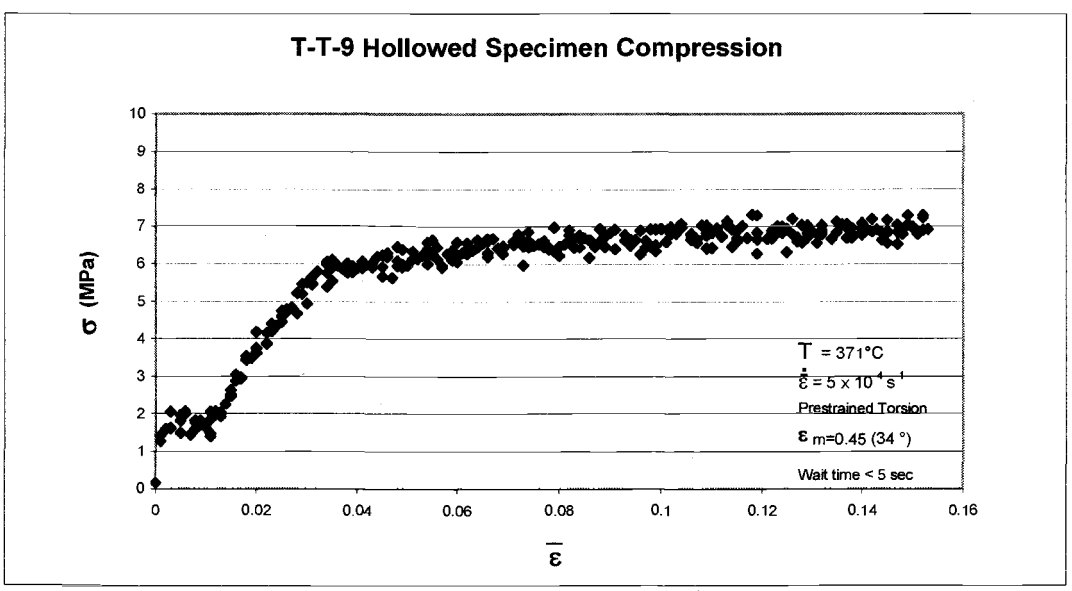
T-T-9 Hollowed Specimen Compression
σ (MPa)
$\bar{\varepsilon}$
T = 371°C
$\dot{\bar{\varepsilon}} = 5 \times 10^{-4}\ s^{-1}$
Prestrained Torsion
ε_m=0.45 (34 °)
Wait time < 5 sec
0
1
2
3
4
5
6
7
8
9
10
0
0.02
0.04
0.06
0.08
0.1
0.12
0.14
0.16

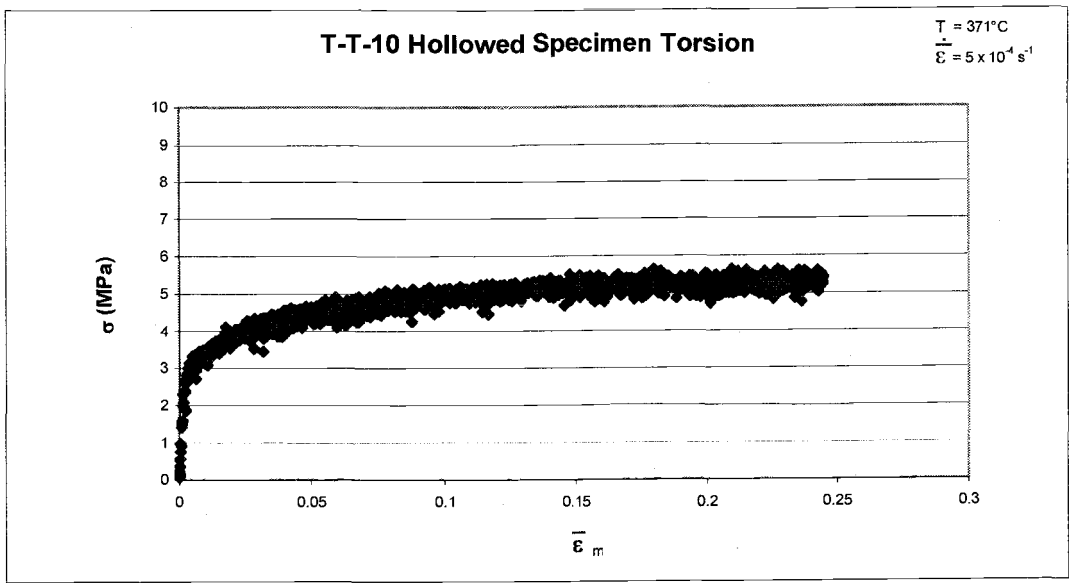
T-T-10 Hollowed Specimen Torsion
T = 371°C
$\dot{\bar{\varepsilon}} = 5 \times 10^{-4}\ s^{-1}$
σ (MPa)
$\bar{\varepsilon}_m$
0
1
2
3
4
5
6
7
8
9
10
0
0.05
0.1
0.15
0.2
0.25
0.3

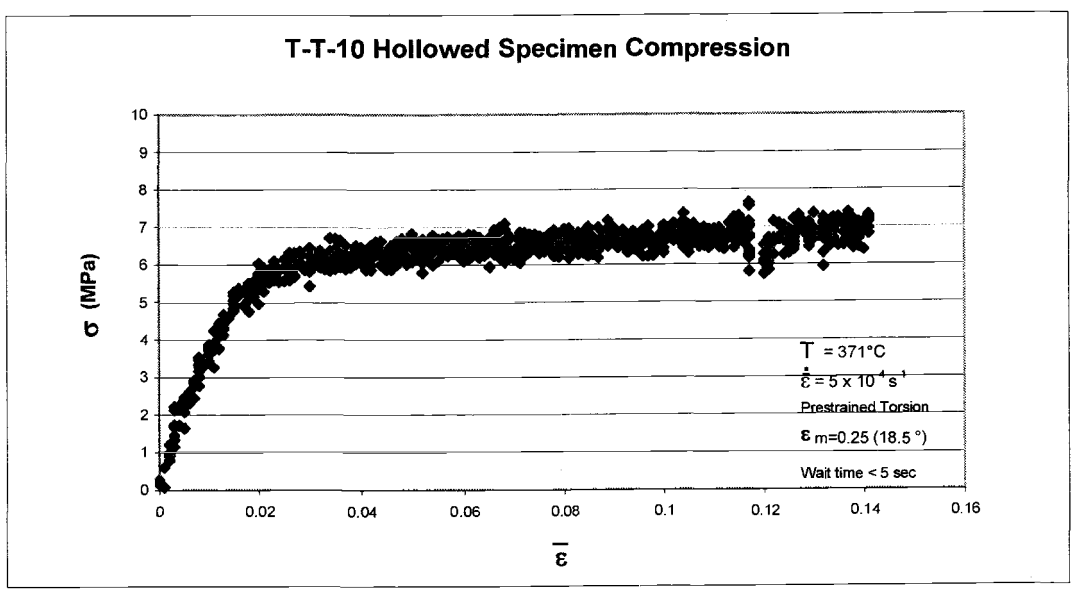
T-T-10 Hollowed Specimen Compression
σ (MPa)
$\bar{\varepsilon}$
T = 371°C
$\dot{\bar{\varepsilon}} = 5 \times 10^{-4}\ s^{-1}$
Prestrained Torsion
ε_m=0.25 (18.5 °)
Wait time < 5 sec
0
1
2
3
4
5
6
7
8
9
10
0
0.02
0.04
0.06
0.08
0.1
0.12
0.14
0.16